# Abrupt transitions in gravity currents

L. A. Amy,[1] A. J. Hogg,[2] J. Peakall,[3] and P. J. Talling[1]

Received 30 June 2004; revised 1 February 2005; accepted 28 February 2005; published 1 July 2005.

[1] Pyroclastic flows and snow avalanches sometimes exhibit a rapid deceleration of their dense flow fronts and detachment of their dilute clouds. This behavior is also inferred for submarine flows and could explain stepped thickness patterns in their deposits. A similar ''abrupt transition'' process occurs in particle-laden, lock release laboratory currents with relatively high concentrations. New experiments on nonparticulate, solute-driven density currents were run to investigate the cause of abrupt transitions. Abrupt transitions occur in laboratory currents with Reynolds numbers (*Re*) less than 1000 and are interpreted, supported by theoretical scaling analysis, to signify a change in dynamic regime. Currents with high *Re*, which do not show abrupt transitions, undergo a downstream change in dynamic regime from (1) inertial slumping to (2) inertial-buoyancy spreading to (3) viscous-buoyancy spreading. In low *Re* currents that undergo abrupt transitions, however, the duration of the second regime is very short, and hence they appear to pass directly from the quickly moving slumping phase into the slowly moving viscous phase. Scaling analysis indicates that an abrupt transition should occur in currents below a critical value of *Re* of $\sim 10-5000$ for currents with different initial aspect ratios. Given that natural flows typically have greater Reynolds numbers, we suggest that abrupt transitions in laboratory and natural currents are likely to be dynamically different. This work has important implications for the physical modeling of gravity flows.

**Citation:** Amy, L. A., A. J. Hogg, J. Peakall, and P. J. Talling (2005), Abrupt transitions in gravity currents, *J. Geophys. Res.*, *110*, F03001, doi:10.1029/2004JF000197.

## 1. Introduction

[2] Gravity currents involve the lateral flow of one fluid into another due to nonuniform fluid density [*Simpson*, 1997; *Kneller and Buckee*, 2000]. Particulate gravity flows, in which the density excess is provided by suspended particles, are common in nature, and include subaqueous sediment gravity flows, pyroclastic flows and powder snow avalanches. These flows pose significant environmental hazards both to human life and infrastructure [see *Simpson*, 1997], while the deposits of ancient submarine flows are important because they host significant volumes of hydrocarbons [*Weimer and Link*, 1991]. An accurate understanding of their flow dynamics is required for both hazard assessment and the prediction of subsurface reservoir characteristics. However, most natural flows are extremely difficult to study directly, especially in submarine environments. Hence indirect methods of study, such as physical laboratory experiments, are an important tool for their analysis.

[3] Sediment gravity flows are commonly generated by catastrophic slope failure. In these cases, mixing occurs with the surrounding fluid at the front and upper boundary of the initial dense flow to produce a vertically stratified current with a relatively dilute overlying ''cloud.'' In pyroclastic density currents the dilute cloud has been observed to outrun its parental high-concentration flow. This behavior is often referred to as ''decoupling'' or ''detachment'' and is associated with rapid deceleration of the dense underflow or interaction of the flow with topography [*Yamamoto et al.*, 1993; *Fisher*, 1995; *Fujii and Nakada*, 1999; *Bourdier and Abdurachman*, 2001; *Cole et al.*, 2002]. A similar type of behavior has also been observed in snow avalanches where a dilute cloud separates from the dense part of the dry snow avalanche, if the latter is rapidly stopped [*Issler*, 2003]. The detachment of mobile dilute clouds can constitute the main hazard in areas prone to subaerial gravity flows [*Bourdier and Abdurachman*, 2001].

[4] Flow transformations from high-concentration (e.g., slides, slumps and debris flows) to low-concentration (e.g., turbidity currents) currents are also envisaged to occur in submarine environments [*Morgenstern*, 1967; *Hampton*, 1972]. Dilution of high-concentration flows has been documented in laboratory experiments [e.g., *van der Knaap and Eijpe*, 1968; *Hampton*, 1972; *Mohrig and Marr*, 2003] and interpreted from the deposits of historical submarine flow events for example, the 1929 Grand Banks event [*Heezen and Ewing*, 1955; *Piper et al.*, 1999], the Orleansville turbidity current [*Heezen and Ewing*, 1955] and the 1979 Nice event [*Mulder et al.*, 1997].

[5] Analog experiments have been used previously to study the motion of density flows [*Schmidt*, 1911; *Keulegan*,

[1]Department of Earth Sciences, Centre for Environmental and Geophysical Flows, University of Bristol, Bristol, UK.
[2]School of Mathematics, Centre for Environmental and Geophysical Flows, University of Bristol, Bristol, UK.
[3]Earth and Biosphere Institute, School of Earth and Environment, University of Leeds, Leeds, UK.


0148-0227/05/2004JF000197$09.00

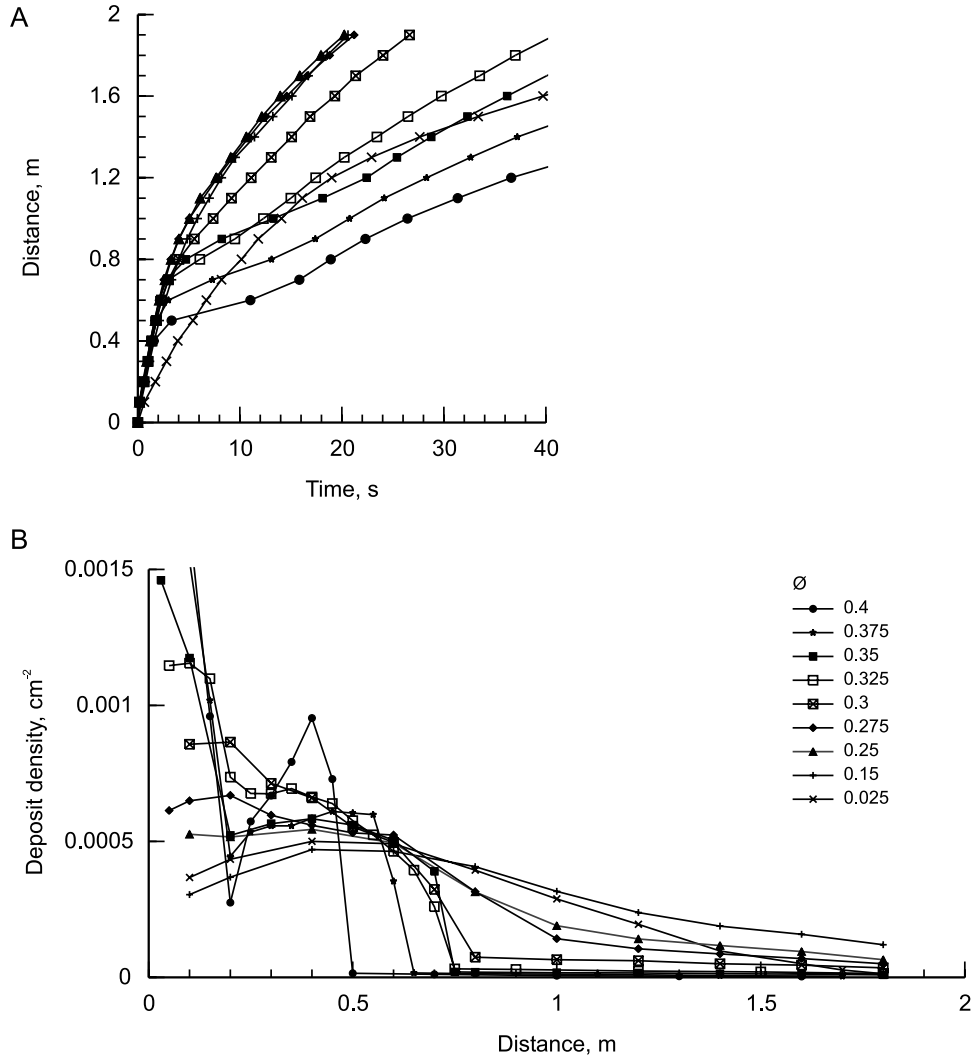


**Figure 1.** Experimental data reported by *Hallworth and Huppert* [1998], showing (a) the position of the flow front as a function of time and (b) the deposit density (mass of particles per unit area) as a function of distance for density currents with varied volume fractions of 9 μm silicon carbide particles. Currents with Ø < 0.275 show a gradual deceleration and decrease in deposit density moving downstream, while those with Ø > 0.275 show a relatively abrupt change in velocity and deposit density moving downstream.

1957; *Rottman and Simpson*, 1983]. A commonly used approach is the lock exchange method, where a volume of relatively dense fluid, contained within a lock, is suddenly released into a larger volume of ambient fluid of a lower density [*Simpson*, 1997]. A number of studies have shown that laboratory flows generated by this method, may undergo similar transformations to those described from nature, involving a rapid deceleration of a relatively dense flow and the detachment of a dilute overlying cloud [*Luthi*, 1981; *Hallworth and Huppert*, 1998; *Choux*, 2001]. *Hallworth and Huppert* [1998] called this behavior an "abrupt transition" and elegantly showed how this behavior is developed at relatively high particle concentrations by running a series of experiments in which they progressively increased the initial particle concentration (Figure 1). They also noted that the abrupt transition produces deposits with a thick proximal layer of fairly constant thickness and a very much thinner distal layer (Figure 1b). The "stepped thickness distribution" of these experimental deposits has been compared to the geometry of beds deposited by turbidity currents [*Kneller and Buckee*, 2000], that may indicate a similar abrupt transition process in submarine environments. Lock exchange flows have been the basis for previous theoretical modeling of surge-type flows [e.g., *Huppert and Simpson*, 1980; *Rottman and Simpson*, 1983; *Klemp et al.*, 1994; *Dade and Huppert*, 1995; *Hallworth and Huppert*, 1998; *Gladstone and Woods*, 2000; *Harris et al.*, 2002]. Despite previous theoretical work, *Hallworth and Huppert* [1998] were unable to explain the abrupt transition behavior of relatively high-concentration flows quantitatively.

[6] In this study we investigate the physical cause of abrupt transitions sensu *Hallworth and Huppert* [1998] in high-concentration laboratory currents using new experimental data. Our motivation was to evaluate if abrupt transitions in laboratory currents are dynamically similar to the abrupt transition-like behavior (i.e., deceleration and

decoupling) of natural currents. In the new experiments the excess buoyancy of the gravity currents was provided by a solution of greater density than the ambient fluid. This approach was followed first because a theoretical treatment of solute-driven density currents is made easier. Secondly, comparison of the results from solute-driven flows (this study) and particle-laden ones (using data from *Hallworth and Huppert* [1998]) has allowed us to test the importance of sedimentation and non-Newtonian rheology on the abrupt transition behavior.

[7] Lock exchange gravity current experiments are described, in which the initial kinematic viscosity and aspect ratio of currents were varied. We find that with increasing kinematic viscosity, currents exhibit transitions that become progressively more abrupt, as was also found by *Hallworth and Huppert* [1998] for increasing initial particle concentration. Scaling analysis is then employed to predict the length and timescales for abrupt transition theoretically. Theory is then compared to the laboratory results of solute-driven flows and particle-driven flows. The agreement between theoretical and laboratory results allows us to propose a physical explanation for abrupt transition in laboratory currents. A number of other key aspects of the behavior of laboratory flows are also analyzed: how does slope gradient affect abrupt transition behavior and what governs the buoyancy and hence strength of the dilute cloud? In the discussion we address whether the abrupt transition behavior of laboratory currents is dynamically similar to those in natural currents.

## 2. Review of Previous Experimental Work

### 2.1. Low-Concentration Flows

[8] The motion of particulate and nonparticulate gravity currents over a horizontal boundary has been extensively studied using simple lock exchange experiments (see references in *Simpson* [1997] and *Kneller and Buckee* [2000]). The propagation of inertial saline flows has been thoroughly investigated to yield a range of theoretical models of their motion. These include direct numerical simulation of the governing equations [*Klemp et al.*, 1994], shallow water models which exploit the low aspect ratio of the flow [*Rottman and Simpson*, 1983] and box models which do not resolve the internal characteristics of currents but provide simple theoretical models for their motion [*Huppert and Simpson*, 1980]. Models have also been developed to describe the motion and deposition from low-concentration, sediment-laden laboratory flows [*Dade and Huppert*, 1995; *Hallworth and Huppert*, 1998; *Gladstone and Woods*, 2000; *Harris et al.*, 2002]. These studies show that inertial, lock exchange gravity currents pass through three distinct flow regimes with increasing time: (1) a slumping phase; (2) an inertial-buoyancy phase; and (3) a viscous-buoyancy phase [*Huppert and Simpson*, 1980; *Rottman and Simpson*, 1983]. Each phase is characterized by a distinct rate of propagation due to different balancing forces. During the initial slumping phase, the length, $x$, of the current is proportional to the time elapsed, $t$. From dimensional analysis,

$$\frac{dx}{dt} = k(g'h_0)^{1/2}, \tag{1}$$

where $g' = g(\rho_f - \rho_a)/\rho_a$, is the reduced gravity, $g$ is gravitational acceleration, $\rho_f$ and $\rho_a$ are the densities of the flow and ambient fluid and $h_0$ is the initial current depth. *Rottman and Simpson* [1983] found values of the constant $k$ of $\sim$0.45 when the initial flow depths and the ambient depth were similar.

[9] After the slump phase the current decelerates with $x$ increasing at a rate proportional to $\sim t^{2/3}$ when there is a balance between inertial and buoyancy forces. For solute flows with low density ratios and in which viscous forces and mixing processes are negligible, the progress of the current during the inertial-buoyancy phase can be modeled as a series of collapsing boxes of a constant area [*Huppert and Simpson*, 1980], so that when the flow depth is much less than the ambient depth,

$$x = (3/2Fr)^{2/3}(g'A)^{1/3}t^{2/3}, \tag{2}$$

where $A$ is the cross-sectional area and $Fr$ is the Froude number at the front of the flow. Theoretical analysis identified a value of $\sqrt{2}$ for the Froude number [*Benjamin*, 1968], whereas laboratory studies have found a slightly lower value of $\sim$1.19 for low-density ratio, lock exchange currents [*Huppert and Simpson*, 1980], when the current's thickness is small compared to the ambient depth. A transition in regimes, from the slump to inertial buoyancy, occurs when a wave, generated on release of the lock gate, has reflected off the back wall of the lock and propagated to the nose of the current [*Rottman and Simpson*, 1983]. This transition distance, $x_s$, has been determined empirically as

$$x_s = x_o(3 + 7.4(h_0/H)), \tag{3}$$

where $x_o$ and $h_0$ are the initial length and height of the dense fluid and $H$ the depth of the ambient fluid. Eventually the effects of viscosity become nonnegligible and the flow enters a new regime, in which the pressure gradient associated with the excess density balances the viscous force. In this regime the length of the current increases as $t^{1/5}$ [*Huppert*, 1982]. Furthermore, the transition from the inertial-buoyancy to viscous-buoyancy phase occurs when

$$x^* = \left(x_0^5 h_0^5 g'/\nu^2\right)^{1/7}, \tag{4}$$

where $\nu$ is the kinematic viscosity [*Huppert*, 1982].

[10] The deposits of low-concentration, particulate-laden flows that undergo this spreading pattern typically produce deposits that gradually decrease in thickness downstream from a maximum close to the release point [e.g., *Bonnecaze et al.*, 1993; *Hallworth and Huppert*, 1998] (Figure 1b). Deposition occurs by particle settling out of suspension and the deposit progressively aggrades with time [*Rooij and Daziel*, 2001].

### 2.2. High-Concentration Flows

[11] *Hallworth and Huppert* [1998] carried out a series of particle-laden lock exchange experiments in which the initial volume fraction of particles (Ø) was increased from 0.009 to 0.432. These experiments showed that currents with relatively high concentrations propagate in a different

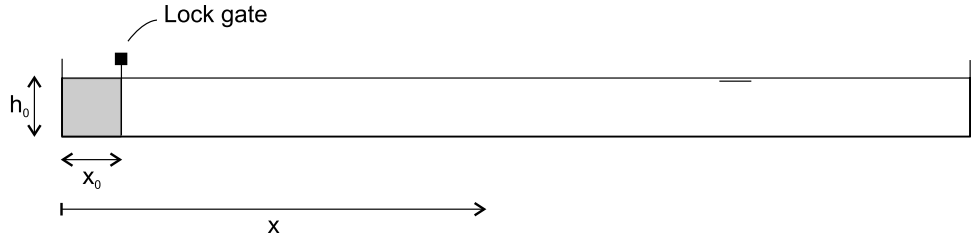


**Figure 2.** Schematic of the lock exchange tank used to generate gravity currents. After raising the lock gate, dense fluid in the lock forms an underflow spreading along the channel.

manner and produce different depositional patterns compared to low-concentration flows (Figure 1). In the case of flows with initial volume fractions of particles greater than 0.275, currents formed rapidly moving, densely compacted flows that came to an abrupt halt. Prior to arrest, a dilute cloud was produced by turbulent mixing at the upper surface of the dense flow. On arrest of the dense flow this cloud decoupled and proceeded downstream. This behavior formed a step in the deposit bed thickness between a relatively thick proximal bed produced by the dense flow and a much thinner distal bed produced by the detached cloud (Figure 1b).

[12] Several other lock exchange studies have also reported abrupt transitions in high-concentration particle-laden currents. *Luthi* [1981] noted the detachment of a dilute cloud from a "very dense slurry which flows like a debris flow" in chalk powder slurries with initial densities of 1.5 g $cm^{-3}$. *Choux* [2001, Figure III.5b] reported flows with Ø of 0.16 and 0.27 that underwent an abrupt deceleration and interpreted this behavior as an effect of high concentrations. Although spreading rates were not described by *Middleton and Neal* [1989, Figure 3], their flows with Ø equal to 0.4 produced deposits with a stepped geometry, suggesting that the parental flows may have experienced an abrupt transition. Beds with stepped profiles were also described by *Choux and Druitt* [2002, Figure 4]. In this case the depositional flows carried particles with two different densities and hence the resulting bed geometry was probably caused by contrasting lateral grading patterns of relatively light and dense particles. Interestingly subaerial granular flows, generated by the sudden collapse of a static cylindrical column of grains, also display an abrupt halt, interpreted to occur when particle frictional forces become dominant [*Lube et al.*, 2004].

[13] *Hallworth and Huppert* [1998] found that existing theoretical models, used to describe low-concentration particulate flows [e.g., *Dade and Huppert*, 1995; *Hallworth and Huppert*, 1998] and based on the assumption that $Ø \ll 1$, offer a poor description of the advance and behavior of relatively high-concentration laboratory flows. They attempted to improve the quantitative interpretation of these models by using a different representation of the reduced gravity expressed by $g'' = g(\rho_f - \rho_a)/\rho_f$. This form of the reduced gravity had been employed for currents with both small and large density ratios (i.e., non-Boussinesq fronts) by *Gröbelbauer et al.* [1993]; using $g''$ makes negligible difference at low-density ratios, but decreases the reduced gravity at higher density ratios. However, *Hallworth and Huppert*'s [1998] analysis showed that adopting the alternative reduced gravity, $g''$, instead of $g'$, was insufficient to improve the agreement between theory and experimental results for their high-concentration experiments.

## 3. Methodology

### 3.1. Experimental Procedure

[14] Solute-driven density flows consisting of aqueous glycerol mixtures (AGS) and aqueous glycerol-sugar solutions (AGSS) were generated. Experiments were run in a perspex channel with a lock located at one end (Figure 2). The channel was filled with tap water to the same depth as the fluid held in the lock. Solutions were thoroughly mixed prior to filling of the lock and contained 15 ml of blue food coloring to aid flow visualization. The density and viscosity of mixtures of AGSS were measured using a digital scale and Haake RS-100 rheometer, respectively. The same properties for AGS mixtures were estimated using data published by *Lide et al.* [2004] (available at http://www.hbcpnetbase.com). The lock gate was rapidly removed allowing the dense fluid to travel as an underflow along the bottom of the channel. During each run the advance of the head was recorded using a digital video camera from which the time, $t$, it took for the flow to advance intervals of 0.1 m was subsequently measured from slow-motion replays.

### 3.2. Experimental Series

[15] The initial conditions of each experiment are listed in Table 1. Six experimental series were conducted, series A0, B0, B1, B3, B5 and C0. Two tanks were used with different lock dimensions. Experiments of series A and B were run in a plastic channel 4.5 m long and 0.2 m wide with a lock 0.1 m long and 0.1 m deep. This channel sat within a larger deep gravity flow tank and on a floor that could be tilted by up to 5°. Those of series C were run in a plastic channel measuring 4.3 m long and 0.2 m wide with a lock 0.34 m long and 0.15 m deep. In series A the density of each solution was kept constant but the viscosity was varied (Figure 3). This was achieved by using varying proportions of aqueous glycerol and aqueous sugar solutions of the same density (1266 ± 6 kg $m^{-3}$). In series B and C aqueous glycerol solutions (AGS) were used. The initial glycerol concentration was systematically increased so that both the viscosity and density of flows were varied. The initial density ratios ($\rho^* = [(\rho_f - \rho_a)/(\rho_f + \rho_a)]^{1/2}$) for all currents varied between 0.1 and 0.35. *Gröbelbauer et al.* [1993] found that the Boussinesq approximation (i.e., variations in density may be neglected as far as they affect inertia) is valid for lock exchange currents with $\rho^* < 0.3$ and that

**Table 1.** Summary of Experiment Conditions and Flow Properties[a]

| Name | Sol. | γ, deg | $x_0$, m | $h_0$, m | $g'$, m s$^{-2}$ | AGS,[b] % | ρ, kg m$^{-3}$ | μ, kg m$^{-1}$ s$^{-1}$ | ν, m$^2$ s$^{-1}$ × 10$^{-6}$ | $u_i$, m s$^{-1}$ | $T_a$, °C | $T_c$, °C | *Re* | *Fr* | *Ri* | ρ* |
|---|---|---|---|---|---|---|---|---|---|---|---|---|---|---|---|---|
| | | | | | | | | *Series A0* | | | | | | | | |
| A0-1[c] | AGSS | 0 | 0.1 | 0.1 | 2.77 | **0** | 1268 | 0.03 | 23.7 | 0.20 | 16.5 | 22 | 845 | 0.38 | 6.94 | 0.35 |
| A0-2[c] | AGSS | 0 | 0.1 | 0.1 | 2.76 | **20** | 1266 | 0.07 | 55.3 | 0.20 | 16.5 | 21 | 362 | 0.38 | 6.89 | 0.35 |
| A0-3[c] | AGSS | 0 | 0.1 | 0.1 | 2.76 | **40** | 1266 | 0.1 | 79.0 | 0.20 | 16 | 19.75 | 253 | 0.38 | 6.89 | 0.35 |
| A0-4[c] | AGSS | 0 | 0.1 | 0.1 | 2.76 | **60** | 1266 | 0.25 | 197.5 | 0.19 | 16 | 20 | 96 | 0.36 | 7.63 | 0.35 |
| A0-5[c] | AGSS | 0 | 0.1 | 0.1 | 2.70 | **80** | 1260 | 0.48 | 380.9 | 0.19 | 15.5 | 20 | 50 | 0.37 | 7.47 | 0.35 |
| | | | | | | | | *Series B0* | | | | | | | | |
| B0-1 | AGS | 0 | 0.1 | 0.1 | 0.22 | 5 | 1010 | 0.001 | 1.3 | 0.05 | 16.0 | 18.8 | 3957 | 0.34 | 8.73 | 0.10 |
| B0-2 | AGS | 0 | 0.1 | 0.1 | 0.75 | 25 | 1064 | 0.002 | 2.1 | 0.10 | 16.0 | 21.0 | 4773 | 0.36 | 7.54 | 0.19 |
| B0-3 | AGS | 0 | 0.1 | 0.1 | 1.42 | 50 | 1131 | 0.006 | 4.9 | 0.15 | 16.0 | 22.3 | 2971 | 0.39 | 6.71 | 0.26 |
| B0-4 | AGS | 0 | 0.1 | 0.1 | 1.95 | 70 | 1185 | 0.017 | 14.3 | 0.17 | 16.0 | 23.3 | 1225 | 0.40 | 6.39 | 0.30 |
| B0-5[c] | AGS | 0 | 0.1 | 0.1 | 2.20 | 80 | 1210 | 0.044 | 36.6 | 0.19 | 16.3 | 23.0 | 520 | 0.40 | 6.10 | 0.32 |
| B0-6[c] | AGS | 0 | 0.1 | 0.1 | 2.36 | 85 | 1226 | 0.071 | 58.3 | 0.19 | 16.0 | 22.5 | 326 | 0.39 | 6.54 | 0.33 |
| B0-7[c] | AGS | 0 | 0.1 | 0.1 | 2.49 | 90 | 1239 | 0.220 | 177.3 | 0.18 | 16.0 | 20.5 | 102 | 0.36 | 7.68 | 0.34 |
| B0-8[c] | AGS | 0 | 0.1 | 0.1 | 2.63 | 95 | 1253 | 0.534 | 425.9 | 0.18 | 16.5 | 19.5 | 42 | 0.35 | 8.11 | 0.34 |
| B0-9[c] | AGS | 0 | 0.1 | 0.1 | 2.70 | 100 | 1260 | 1.629 | 1292.6 | 0.14 | 16.0 | 18.8 | 11 | 0.27 | 13.77 | 0.35 |
| | | | | | | | | *Series B1* | | | | | | | | |
| B1-1 | AGS | 1 | 0.1 | 0.1 | 0.22 | 5 | 1010 | 0.001 | 1.3 | 0.04 | 17.8 | 19.0 | 3542 | 0.30 | . . . | 0.10 |
| B1-2 | AGS | 1 | 0.1 | 0.1 | 0.75 | 25 | 1064 | 0.002 | 2.1 | 0.11 | 17.7 | 21.6 | 5042 | 0.38 | . . . | 0.19 |
| B1-3 | AGS | 1 | 0.1 | 0.1 | 1.42 | 50 | 1131 | 0.005 | 4.7 | 0.15 | 18.0 | 23.3 | 3125 | 0.39 | . . . | 0.26 |
| B1-4[c] | AGS | 1 | 0.1 | 0.1 | 1.95 | 70 | 1185 | 0.016 | 13.8 | 0.17 | 17.9 | 23.6 | 1266 | 0.40 | . . . | 0.30 |
| B1-5[c] | AGS | 1 | 0.1 | 0.1 | 2.20 | 80 | 1210 | 0.043 | 35.6 | 0.19 | 17.9 | 23.3 | 525 | 0.40 | . . . | 0.32 |
| B1-6[c] | AGS | 1 | 0.1 | 0.1 | 2.36 | 85 | 1226 | 0.071 | 57.8 | 0.19 | 18.0 | 22.6 | 328 | 0.39 | . . . | 0.33 |
| B1-7[c] | AGS | 1 | 0.1 | 0.1 | 2.49 | 90 | 1239 | 0.203 | 163.5 | 0.19 | 18.0 | 22.1 | 115 | 0.38 | . . . | 0.34 |
| B1-8[c] | AGS | 1 | 0.1 | 0.1 | 2.63 | 95 | 1253 | 0.511 | 408.0 | 0.17 | 18.1 | 20.8 | 43 | 0.34 | . . . | 0.34 |
| B1-9[c] | AGS | 1 | 0.1 | 0.1 | 2.70 | 100 | 1260 | 1.599 | 1269.4 | 0.13 | 18.2 | 19.8 | 10 | 0.25 | . . . | 0.35 |
| | | | | | | | | *Series B3* | | | | | | | | |
| B3-1 | AGS | 3 | 0.1 | 0.1 | 0.22 | 5 | 1010 | 0.001 | 1.3 | 0.05 | 14.7 | 18.4 | 3970 | 0.34 | . . . | 0.10 |
| B3-2 | AGS | 3 | 0.1 | 0.1 | 0.75 | 25 | 1064 | 0.002 | 2.1 | 0.11 | 13.6 | 19.9 | 5270 | 0.41 | . . . | 0.19 |
| B3-3 | AGS | 3 | 0.1 | 0.1 | 1.42 | 50 | 1131 | 0.006 | 5.5 | 0.17 | 14.6 | 19.3 | 3118 | 0.45 | . . . | 0.26 |
| B3-4 | AGS | 3 | 0.1 | 0.1 | 1.95 | 70 | 1185 | 0.018 | 15.5 | 0.20 | 13.2 | 22.3 | 1309 | 0.46 | . . . | 0.30 |
| B3-5[c] | AGS | 3 | 0.1 | 0.1 | 2.20 | 80 | 1210 | 0.051 | 42.3 | 0.21 | 13.1 | 21.3 | 488 | 0.44 | . . . | 0.32 |
| B3-6[c] | AGS | 3 | 0.1 | 0.1 | 2.36 | 85 | 1226 | 0.088 | 72.0 | 0.21 | 13.2 | 20.0 | 294 | 0.44 | . . . | 0.33 |
| B3-7[c] | AGS | 3 | 0.1 | 0.1 | 2.49 | 90 | 1239 | 0.226 | 182.5 | 0.20 | 14.2 | 19.9 | 110 | 0.40 | . . . | 0.34 |
| B3-8[c] | AGS | 3 | 0.1 | 0.1 | 2.63 | 95 | 1253 | 0.548 | 437.6 | 0.20 | 13.7 | 18.7 | 45 | 0.38 | . . . | 0.34 |
| B3-9[c] | AGS | 3 | 0.1 | 0.1 | 2.70 | 100 | 1260 | 1.594 | 1264.9 | 0.18 | 13.5 | 19.0 | 14 | 0.34 | . . . | 0.35 |
| | | | | | | | | *Series B5* | | | | | | | | |
| B5-1 | AGS | 5 | 0.1 | 0.1 | 0.22 | 5 | 1010 | 0.001 | 1.3 | 0.05 | 14.0 | 17.7 | 4103 | 0.35 | . . . | 0.10 |
| B5-2 | AGS | 5 | 0.1 | 0.1 | 0.75 | 25 | 1064 | 0.002 | 2.2 | 0.13 | 13.4 | 17.9 | 5795 | 0.46 | . . . | 0.19 |
| B5-3 | AGS | 5 | 0.1 | 0.1 | 1.42 | 50 | 1131 | 0.006 | 5.4 | 0.18 | 13.2 | 19.7 | 3294 | 0.47 | . . . | 0.26 |
| B5-4 | AGS | 5 | 0.1 | 0.1 | 1.95 | 70 | 1185 | 0.020 | 17.0 | 0.21 | 13.3 | 21.2 | 1254 | 0.48 | . . . | 0.30 |
| B5-5[c] | AGS | 5 | 0.1 | 0.1 | 2.20 | 80 | 1210 | 0.048 | 39.9 | 0.21 | 15.5 | 22.0 | 535 | 0.46 | . . . | 0.32 |
| B5-6[c] | AGS | 5 | 0.1 | 0.1 | 2.36 | 85 | 1226 | 0.078 | 63.7 | 0.23 | 15.5 | 21.5 | 360 | 0.47 | . . . | 0.33 |
| B5-7[c] | AGS | 5 | 0.1 | 0.1 | 2.49 | 90 | 1239 | 0.236 | 190.2 | 0.23 | 13.8 | 19.0 | 121 | 0.46 | . . . | 0.34 |
| B5-8[c] | AGS | 5 | 0.1 | 0.1 | 2.63 | 95 | 1253 | 0.516 | 412.1 | 0.24 | 17.5 | 20.5 | 59 | 0.47 | . . . | 0.34 |
| B5-9[c] | AGS | 5 | 0.1 | 0.1 | 2.70 | 100 | 1260 | 1.630 | 1293.7 | 0.19 | 13.7 | 18.7 | 15 | 0.37 | . . . | 0.35 |
| | | | | | | | | *Series C0* | | | | | | | | |
| C0-1 | AGS | 0 | 0.34 | 0.15 | 0.22 | 5 | 1010 | 0.001 | 1.3 | 0.05 | 7 | 8 | 5718 | 0.28 | 13.09 | 0.10 |
| C0-2 | AGS | 0 | 0.34 | 0.15 | 0.75 | 25 | 1064 | 0.002 | 2.2 | 0.12 | 7.5 | 14 | 7782 | 0.36 | 7.85 | 0.19 |
| C0-3 | AGS | 0 | 0.34 | 0.15 | 1.42 | 50 | 1131 | 0.007 | 6.0 | 0.17 | 8.5 | 17 | 4209 | 0.37 | 7.36 | 0.26 |
| C0-4 | AGS | 0 | 0.34 | 0.15 | 1.95 | 70 | 1185 | 0.020 | 17.2 | 0.20 | 9 | 21 | 1727 | 0.37 | 7.33 | 0.30 |
| C0-5[c] | AGS | 0 | 0.34 | 0.15 | 2.20 | 80 | 1210 | 0.057 | 46.7 | 0.21 | 12 | 20 | 679 | 0.37 | 7.49 | 0.32 |
| C0-6[c] | AGS | 0 | 0.34 | 0.15 | 2.36 | 85 | 1226 | 0.088 | 71.8 | 0.22 | 11 | 20 | 458 | 0.37 | 7.32 | 0.33 |
| C0-7[c] | AGS | 0 | 0.34 | 0.15 | 2.49 | 90 | 1239 | 0.225 | 181.6 | 0.23 | 9 | 20 | 186 | 0.38 | 7.06 | 0.34 |
| C0-8[c] | AGS | 0 | 0.34 | 0.15 | 2.63 | 95 | 1253 | 0.508 | 405.2 | 0.23 | 7.5 | 21 | 86 | 0.37 | 7.45 | 0.34 |
| C0-9[c] | AGS | 0 | 0.34 | 0.15 | 2.70 | 100 | 1260 | 1.594 | 1264.9 | 0.24 | 8 | 20 | 28 | 0.38 | 7.03 | 0.35 |

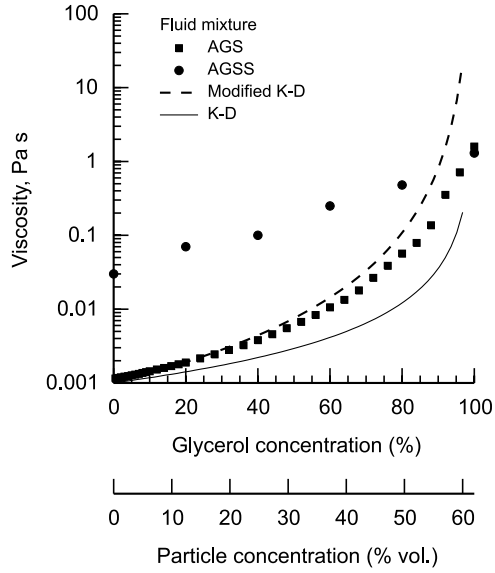


**Figure 3.** Viscosity as a function of concentration for glycerol solutions and particle-water slurries. The concentration of aqueous glycerol solutions (AGS) and aqueous sugar-glycerol solutions (AGSS) is given by weight percent and volume percent, respectively. Data for AGS is from *Lide et al.* [2004] and those for AGSS are from measurements obtained using a Haake rotational viscometer. The *Kreieger and Dougherty* [1959] model (K-D) describes the viscosity of suspensions composed of water and noncohesive hard spheres. A modified K-D model is also shown, established by measurements of silicon carbide slurries composed of particles with an average size of 13 μm and at shear rates of ∼100 $s^{-1}$ [*Ferreira and Diz*, 1999].

flows became increasingly non-Boussinesq as $\rho^* \rightarrow 1$. Thus the high-density ratio experiments of this study were non-Boussinesq ($\rho^* > 0.3$), although probably only weakly, in view of the results of *Gröbelbauer et al.* [1993].

### 3.3. Solution Properties

[16] Glycerol solutions were used in this study since they have broadly similar properties to particle-laden mixtures. For both AGS and particle-water mixtures, viscosity increases with concentration, whereby at relatively high particle concentrations small changes of concentration result in large differences in viscosity [*Lide et al.*, 2004]. Viscosity varies from $10^{-3}$ to 1.5 kg $m^{-1}$ $s^{-1}$ for minimum and maximum glycerol concentrations. Similar ranges in viscosity exist for certain mixtures of sediment and water (Figure 3) including those silicon carbide slurries used by *Hallworth and Huppert* [1998]. Sediment-water mixtures comprising noncohesive sediment of a wide range of particle sizes display shear stresses proportional to shear rates up to concentrations of $\emptyset \sim 0.5$, close to the maximum packing density of ∼0.6 for monodisperse spheres [*Barnes*, 1989]. In this respect the Newtonian solutions used in this study are comparable to noncohesive sediment-water mixtures. However, sediment-water mixtures are strictly non-Newtonian due to the presence of normal stresses produced by particle interaction [*Bagnold*, 1954]. Also, mixtures containing cohesive particles may exhibit non-Newtonian properties at relatively low sediment concentrations [*Major and Pierson*, 1992; *Coussot*, 1997]. Hence the properties of cohesive sediment-water mixtures may differ significantly from those of the Newtonian solutions used in this study.

## 4. Experimental Results

[17] Once the lock gate was removed, the dense fluid collapsed out and formed a density-driven underflow with a characteristic head, body and tail structure (Figure 4). Calculated Reynolds numbers for the initial flow motion vary from ∼4000 for flows with low viscosities to <50 for those with the highest viscosities (Table 1), indicating a range of flow conditions from turbulent, $Re > 2000$, to laminar, $Re < 500$. Results from experiments using a horizontal channel are presented first, followed by those of experiments using an inclined channel.

### 4.1. Flows Without Abrupt Transitions

[18] Currents with kinematic viscosity less than ∼15 × $10^{-6}$ $m^2$ $s^{-1}$, which correspond to those with $Re > 2000$, exhibited a smooth reduction in head velocity as they propagated along the tank (Figures 4a and 5a). These currents exhibited a turbulent upper boundary with Kelvin-Helmholtz billows produced by shear between the flow and ambient fluid (Figure 4a). Gradual changes in the concentration of the flow front also occurred, as assessed visually from changes in coloration. First, the current's length increased linearly with time, following the prediction of equation (1) (Figure 6). A value for the constant $k \sim 0.4$ was found for the initial slumping stage in which the velocity of the head is constant and similar to that found by *Rottman and Simpson* [1983]. After the slumping stage, the current's length, $x$, increased by $\sim t^{2/3}$ (equation (2)) and then later by $\sim t^{1/5}$. The transition distance from the slumping phase to the inertial-buoyancy phase ($x_s$) occurred at about ten lock lengths, in agreement with equation (3).

### 4.2. Flows With Abrupt Transitions

[19] Flows with kinematic viscosities greater than ∼20 × $10^{-6}$ $m^2$ $s^{-1}$, which correspond to those with $Re < 2000$, displayed an abrupt change in flow velocity and concentration (Figures 4b, 4c, and 5b). Their behavior is similar to the

*Notes to Table 1:*

[a]Variables are the channel slope gradient (γ), lock length ($x_0$) and height ($h_0$), reduced gravity ($g'$), percentage of glycerol (AGS), density (ρ), viscosity (μ), kinematic viscosity (ν), average flow velocity of the flow front in the first 0.5 m ($u_i$), temperature of the ambient fluid ($T_a$) and the current ($T_c$), calculated Reynolds (*Re*), Froude (*Fr*), and Richardson (*Ri*) numbers, and the density ratio (ρ*). The viscosity of aqueous glycerol solutions was corrected for flow temperature ($T_f$) using the empirically derived equation by *Chen and Pearlstein* [1987]. The Reynolds number indicates the relative importance of inertial to viscous forces and has here been calculated using $Re = \rho h_0 u_i / \mu$. Reynolds numbers <500 indicate laminar flow and those >2000 indicate turbulent flow conditions. The Froude number indicates the relative importance of inertial to gravitational forces, calculated here using $Fr = u_i/(g' h_0)^{0.5}$. The inverse of the Froude number, known as the Richardson number, $Ri = g' h_0 / u_i^2$, is also shown. All flows in this study were subcritical indicated by $Fr < 1$.

[b]Values of glycerol are given in percentage by weight, except those in boldface, which are percentage by volume.

[c]Currents that exhibited an abrupt transition.

"abrupt transition" process described by *Hallworth and Huppert* [1998]. At some point in the channel these currents were observed to thin and decelerate rapidly (Figure 4b at $t = 6-8$). A dilute cloud produced by mixing with the ambient fluid was then observed to overtake the dense flow front (Figure 4b at $t = 10$). Overtaking occurred almost instantaneously in currents with relatively low viscosities where the cloud was relatively fast moving and voluminous (e.g., experiments A0-1 and B0-4). In experiments using relatively viscous releases (e.g., experiments A0-5 and B0-8), a delay of some tens of seconds occurred prior to overtaking by a relatively small volume and slowly moving cloud. In this case the cloud was observed to originate from behind the abruptly slowed flow front and to gradually increase in thickness and velocity. The cloud propagated relatively slowly downstream from the transition point developing a distinct head as it moved (Figure 4b at $t = 10-20$). The unmixed fluid was left behind within the body of the current and on close inspection was observed to creep very slowly, $<1$ cm $s^{-1}$. The current with the highest viscosity (experiment B0-9) exhibited little mixing after release and thus did not generate a dilute cloud (Figure 4c). The abrupt transition in this current thus terminated its motion, ignoring subsequent creep.

[20] The abrupt change in front velocity of currents compared to the gentle deceleration of currents with lower viscosities is clearly shown by plotting the mean velocity of the head against the position of the flow front (Figure 5). The abrupt transitions occurred between 10 and 15 lock lengths and became more marked and closer to the source with increasing kinematic viscosity of the released fluid. After the abrupt deceleration, however, the front of some currents was observed to accelerate and reached a similar velocity to currents that did not exhibit an abrupt transition (Figure 5b). Flows that display an abrupt transition deviate significantly from the time-distance path for low-concentration flows (Figure 6). The use of $g''$, proposed by *Gröbelbauer et al.* [1993], for flow with relatively high-density ratios (i.e., non-Boussinesq), instead of $g'$ does not improve the prediction. The spreading pattern of the flow front of currents that undergo an abrupt transition can be partitioned into four stages (Figure 6). First, the current's length increases linearly with time, again following the prediction of equation (1). (For currents with Reynolds numbers <1000, the value of $k$ decreases from values of $\sim 0.4-0.25$ as $Re$ decreases from $\sim 1000$ to $\sim 10$). This pattern of motion is terminated by the abrupt transition, after which the current's length first increases with $\sim t^{1/5}$ for a relatively short period of time, followed by $\sim t^{2/3}$. In the final stages of the flow the current's length increases at $\sim t^{1/5}$.

### 4.3. Currents Flowing Down an Incline

[21] The same two types of flow behavior were observed in experiments where the channel was inclined; currents with relatively low viscosities exhibited a smooth change in velocity and concentration, whereas those with relatively high viscosities exhibited abrupt changes in velocity and concentration (Figure 7). Slope gradient was observed to enhance the amount of mixing in currents. Although increasing the channel gradient did not increase the maximum current velocity significantly, it did influence their deceleration pattern (Figure 7). The transition distance between inertial slumping and inertial-buoyancy spreading and the abrupt transition distance, in high-concentration flows, increased with gradient (Figures 7c and 7e).

### 4.4. Summary of Observations

[22] A distinct change in density current motion with increasing glycerol concentration can be identified for experimental series B and C (Figure 8). Low-concentration flows decelerate gradually downstream after the initial inertial-slumping regime (Figure 8, flow 1). Currents with slightly higher concentrations travel faster, due to their higher excess density, but deceleration occurs in the same manner (Figure 8, flow 2). At higher concentrations, although currents initially go faster, flows undergo an abrupt deceleration. In these flows, the slowly moving, high-concentration front is overtaken almost immediately by a dilute cloud composed of fluid previously in the upper mixed part of the current (Figure 8, flow 3). As concentration is increased further, the abrupt deceleration becomes more pronounced and occurs closer to the point of release. It also takes longer for the dilute cloud to overtake the decelerated high-concentration front (Figure 8, flow 4). At the highest concentration, flows do not develop a cloud due to negligible mixing (Figure 8, flow 5). Experiments of series A0 also showed this change in behavior with increasing initial viscosity, although, the lowest concentration type behavior was not seen since viscosity was relatively high in all A0 experiments.

[23] The abrupt transition represents two processes: (1) the abrupt deceleration of high-concentration fluid and (2) the overtaking of the high-concentration base by low-concentration fluid from the mixed upper part of the flow. Each process is now discussed. Results from the present study are then compared to experimental data from particle-laden flows to assess their dynamic similarity. The dynamic similarity of natural sized flows to laboratory currents is then assessed.

## 5. Analysis and Discussion of Results

### 5.1. Abrupt Transition Occurrence and Location

[24] We interpret the abrupt transitions of these gravity-driven flows to signify a change in their dynamical regimes; in particular, the deceleration signifies that the currents have become viscously controlled. We observed abrupt transitions for currents with Reynolds numbers, based on initial flow depth and initial velocity, of order 1000. As these currents propagate and thin, the viscous stresses

**Figure 4.** Drawings based on photographs showing the progress of glycerol currents. The dashed line indicates the approximate boundary between relatively dense high-concentration fluid and the overlying diluted cloud. (a) A current of 50% AGS that shows a gradual reduction in head velocity and significant mixing at the upper turbulent boundary. (b) A current of 85% glycerol that shows an abrupt transition after about 8 s and subsequent detachment of the low-concentration dilute cloud. (c) A current of 100% glycerol that shows an abrupt transition at an earlier time compared to the 85% glycerol current. This current showed little mixing and therefore did not produce a dilute cloud.

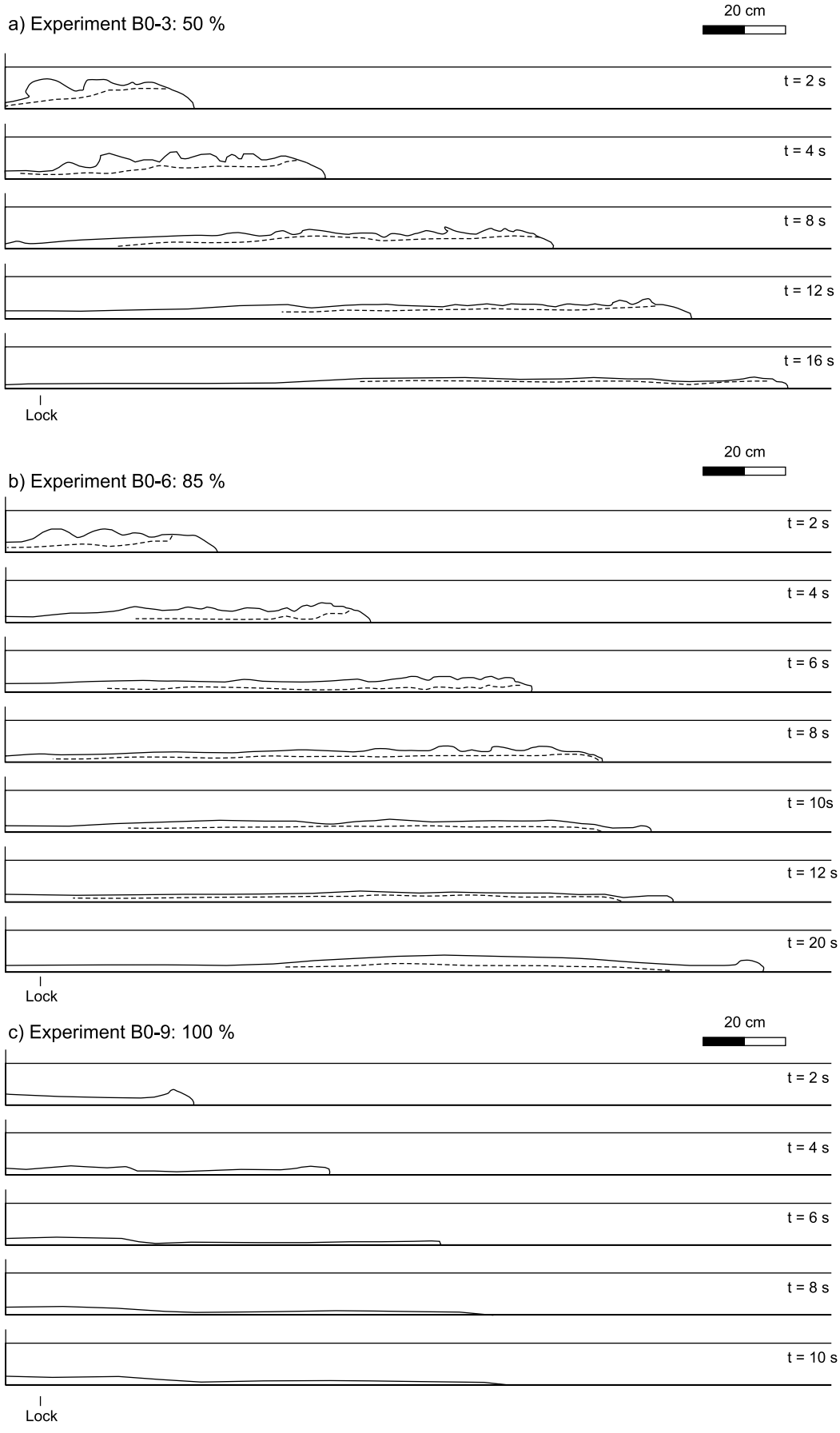
a) Experiment B0-3: 50 %
20 cm
t = 2 s
t = 4 s
t = 8 s
t = 12 s
t = 16 s
Lock
b) Experiment B0-6: 85 %
20 cm
t = 2 s
t = 4 s
t = 6 s
t = 8 s
t = 10s
t = 12 s
t = 20 s
Lock
c) Experiment B0-9: 100 %
20 cm
t = 2 s
t = 4 s
t = 6 s
t = 8 s
t = 10 s
Lock

**Figure 4**

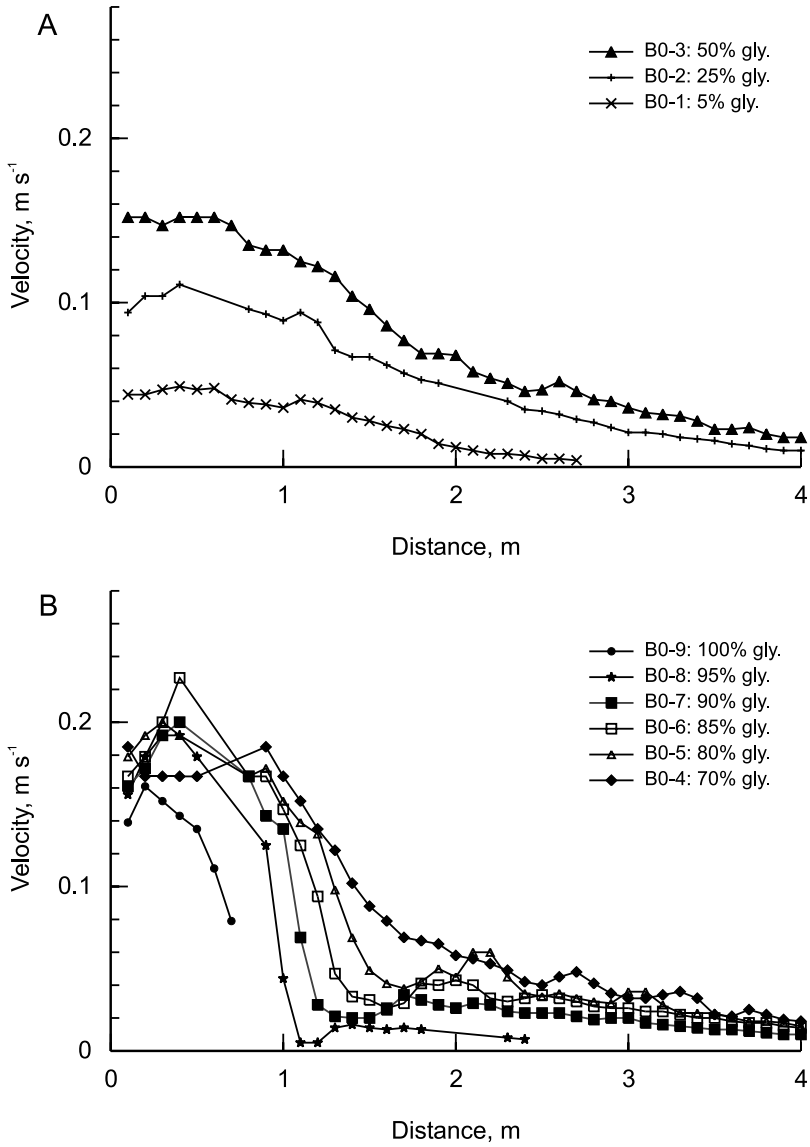


**Figure 5.** Mean head velocities of currents with (a) high (>2000) Reynolds numbers and (b) low (<2000) Reynolds numbers. Data from experiments of series B0. Velocities are averaged over two successive measurements to give a mean value over 10 cm.

developed within them become nonnegligible. Previous investigations have indicated that the change of regimes from inertial-slumping to inertial-buoyancy spreading occurs at distances given by equation (3) [*Rottman and Simpson*, 1983] and this is in accord with our observations of those flows with relatively high initial Reynolds numbers ($Re > 2000$). However, we have observed abrupt transitions at distances less than that given by equation (3). This is consistent with the flow regime changing directly from inertial slumping to viscous-buoyancy spreading, also suggested by the length of the current increasing by $t^{1/5}$ within the latter regime.

[25] Scaling analysis may be usefully employed to differentiate between these various dynamical regimes and to establish the distance at which the abrupt transition may occur. This analysis cannot determine a precise quantitative expression for the abrupt transition, but reveals how the transition distance and other quantities depend upon dimensional properties of the flow. The flow is driven by the pressure gradient associated with the density difference between the intruding and the ambient fluid. The magnitude of the pressure gradient is $\rho g' h/x$, where $h$ and $x$ are the height and length of the current, respectively. Initially the height is comparable with the initial height of the current behind the lock gate, $h_0$, but after it has flowed for sometime, conservation of mass implies that $xh \sim A$, where $A$ is the volume per unit width (which is approximately constant throughout the motion). The pressure gradient is balanced by the rate of change of the inertia of the flow, $\rho u^2/x$, and the divergence of the viscous stresses, $\rho \nu u/h^2$. In this scaling analysis we examine dynamical regimes in which the motion is controlled by a balance between these two dominant physical processes and we investigate the transition between these regimes. This approach is akin to asymptotic analysis of the full governing equations in which various distinguished limits are elucidated. Initially, the

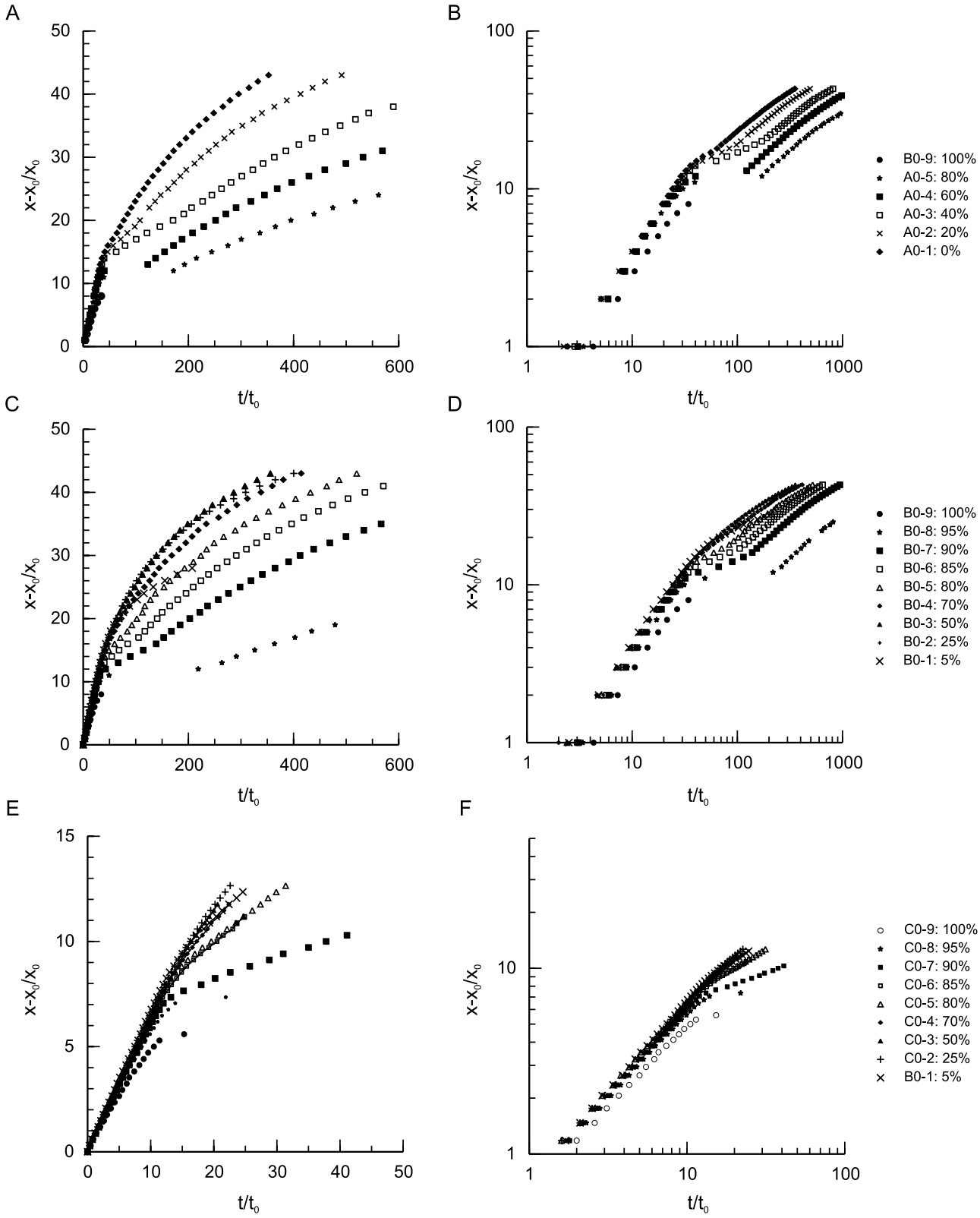


**Figure 6.** Position of the flow front as a function of time for experimental currents of (a, b) series A0, (c, d) series B0, and (e, f) series C0. Graphs show nondimensional values plotted on (left) linear and (right) log axes. The distance from the lock gate to the head of the current, $x$, is nondimensionalized with respect to the lock length, $x_0$, and time after the release of the lock gate, $t$, is nondimensionalized with respect to $t_0 = x_0/(g'h_0)^{1/2}$. This is the same approach used by *Rottman and Simpson* [1983].

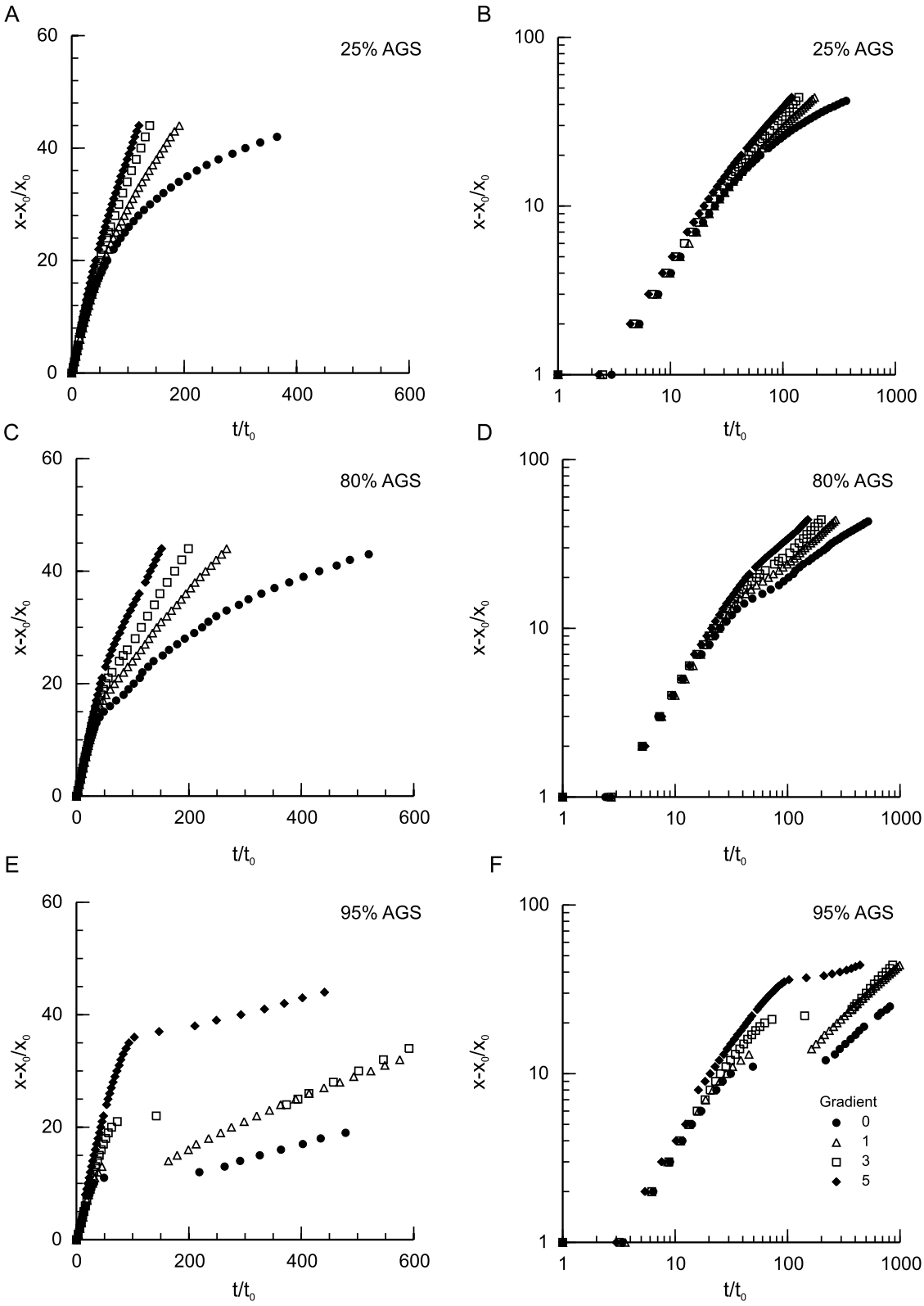


**Figure 7.** Position of the flow front as a function of time for glycerol flows with concentrations of (a, b) 25%, (c, d) 80%, and (e, f) 95% in experiments where the slope gradient was varied. Data are from series B0, B1, B3, and B5. Graphs show nondimensional values plotted on (left) linear and (right) log axes. Values of time and distance are nondimensionalized in the same manner as in Figure 6.

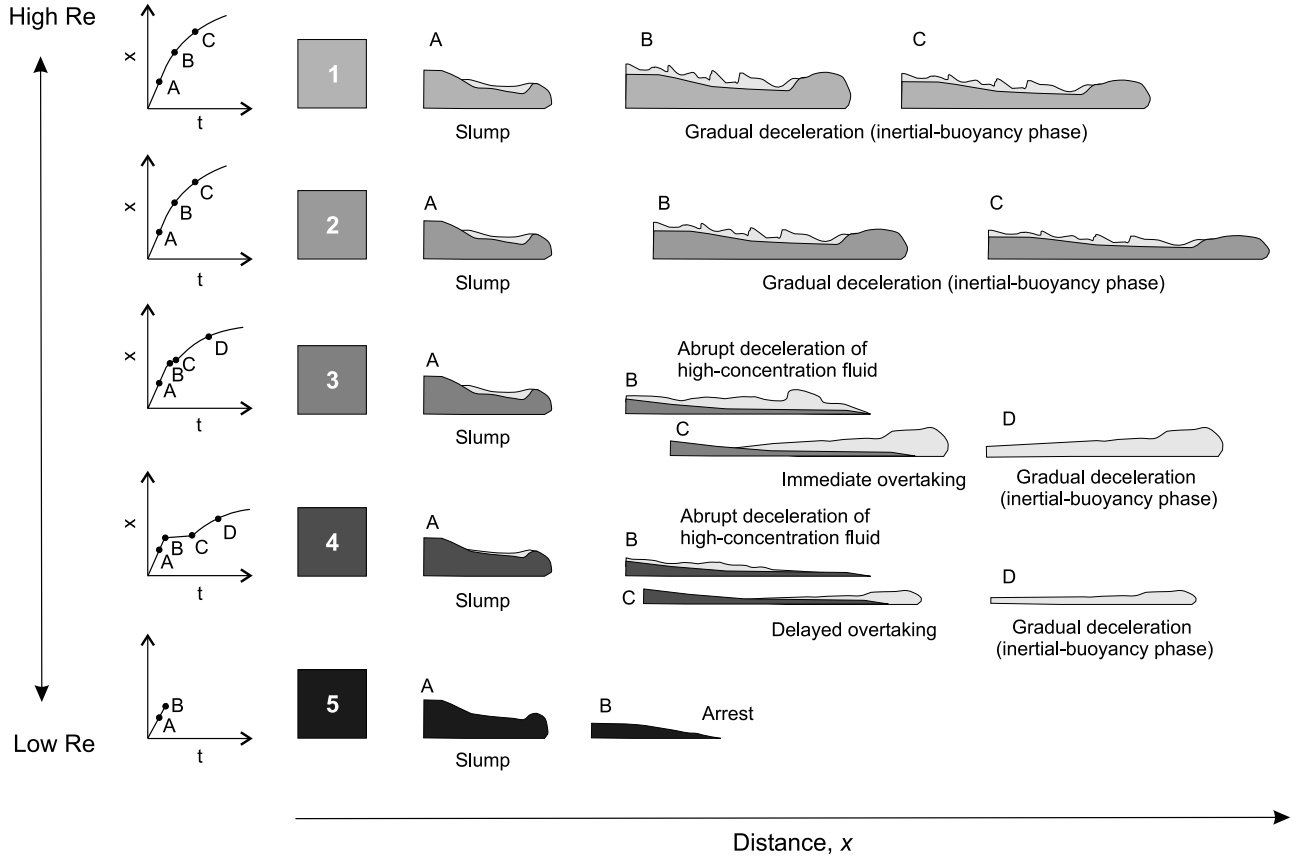


**Figure 8.** Schematic of the different types of current spreading pattern observed in experiments. Characteristic time-distance plots are shown on the left, with black dots marking stages in the flow's development. See text for further explanation.

buoyancy-induced pressure gradient balances the fluid inertia. This yields the slumping regime in which $\rho g' h_0/x \sim \rho x/t^2$. Thus we expect that the length of the current increases as

$$x \sim (g' h_0)^{1/2} t. \tag{5}$$

This regime was established by *Rottman and Simpson* [1983] and is observed in our experiments. Thereafter the inertia-buoyancy regime arises when the current has thinned sufficiently so that its height scale is now given by $A/x$. Thus the balance of the forces imply that $\rho g' A/x^2 \sim \rho x/t^2$ and so

$$x \sim (g' A)^{1/3} t^{2/3}. \tag{6}$$

Alternatively, the viscous-buoyancy regime may occur and this leads to $\rho g' A/x^2 \sim \rho \nu u^3/A^2$ which implies that

$$x \sim \left(g' A^3 t/\nu\right)^{1/5}. \tag{7}$$

Both of these relationships were predicted by *Huppert and Simpson* [1980].

[26] The usual progression of dynamical regimes for most high Reynolds number currents is that first the current follows inertial slumping, followed by a balance of inertial-buoyancy forces and finally a balance between viscous and buoyancy forces. The timescales and length scales at which transitions between regimes occur may be estimated by simultaneously solving the relevant pairs of spreading laws. Thus the transition between inertial slumping and inertial-buoyancy spreading occurs when

$$t_1 \sim A/\left[h_0 (g' h_0)^{1/2}\right] \qquad x_1 \sim A/h_0. \tag{8}$$

Notice that this transition distance is in accord with equation (3) with a premultiplicative constant of order 10 for flows with an initial height equal to the inertial flow depth. Alternatively the transition timescales and length scales between the inertia-buoyancy and viscous-buoyancy phase were deduced by *Huppert* [1982] and are equal to

$$t_2 \sim \left(\frac{A^4}{\nu^3 g'^2}\right)^{1/7} \qquad x_2 \sim \left(\frac{g' A^5}{\nu^2}\right)^{1/7}. \tag{9}$$

[27] A convenient way of following the change in these dynamical regimes is shown in Figure 9a (which is after *Rottman and Simpson* [1983]). For early times ($t \ll t_1$), the flow is slumping inertially and its length grows linearly with time. For intermediate times ($t_1 \ll t \ll t_2$) the flow is in the self-similar inertial-buoyancy phase and the length increases as $t^{2/3}$. Finally at times ($t \gg t_2$), the

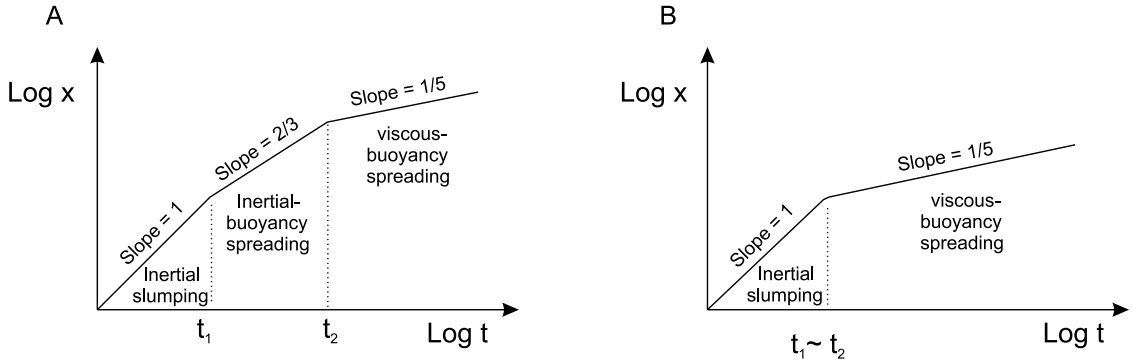


**Figure 9.** Schematic of the change in length of a gravity current with time on log axes. The change in gradient of the line indicates the transition from one dynamical regime to another. The time of transition between inertial slumping and inertial-buoyancy spreading ($t_1$) and inertial-buoyancy spreading and viscous-buoyancy spreading ($t_2$) are shown. The two plots show currents in which (a) $t_1 \ll t_2$ and (b) $t_1 \sim t_2$.

flow is controlled by viscous and buoyancy forces and the length grows as $t^{1/5}$. The transition between each of these regimes is often found to be rapid [*Rottman and Simpson*, 1983].

[28] In this study we found some flows that appear to undergo an abrupt transition from the inertial slumping to the viscous-buoyancy phase. We suggest that this occurs when the two timescales, $t_1$ and $t_2$, are comparable so that the self-similar inertial-buoyancy phase is not observed (Figure 9b). In this case, the abrupt transition should occur at length scales of magnitude $(g'A^5/\nu^2)^{1/7}$. In Figure 10 the nondimensional distance at which the abrupt transition occurs as a function of this parameter is shown. A linear relationship between the two parameters and consistent results for experimental series A and B that employed fluids of rather different density and viscosity are found. The ratio of the two timescales is given by

$$\frac{t_1}{t_2} \sim \left( \frac{(g'h_0)^{1/2} h_0}{\nu} \frac{h_0}{x_0} \right)^{3/7}. \tag{10}$$

Since the initial velocity scale of the motion is $(g'h_0)^{1/2}$ and $\alpha_0 = h_0/x_0$ is the initial aspect ratio, this analysis indicates that the timescales are comparable when

$$[\alpha_0 Re]^{3/7} \sim 1. \tag{11}$$

In these experiments the aspect ratio of the release was kept constant. Thus we anticipate that flows with relatively high Reynolds numbers will not exhibit abrupt transitions, whereas those with sufficiently small Reynolds numbers may and this is in accord with our experimental observations. Scaling relationships, such as those developed above, cannot provide the magnitude of multiplicative constant that relates the length and timescales to the other dimensional properties. However, if we assume that $t_1 = 10A/(h_0(g'h_0)^{1/2})$ [*Rottman and Simpson*, 1983] and that the factor multiplying the parameter in equation (9) is order unity then we would expect first to observe abrupt transitions when $\alpha_0 Re \sim 10^{7/3}$. Using this criterion, abrupt transitions should first be observed in currents of series A0, B0 and C0 at low Reynolds numbers of order 200–500 and this is consistent with the laboratory results (Table 2).

### 5.2. Dynamic Similarity of Particle-Laden Laboratory Currents

[29] The motion of the flow fronts of glycerol flows described in this study exhibit similar patterns to those of particle-laden flows reported by *Hallworth and Huppert* [1998] (Figure 1). A linear relationship is found between the abrupt transition distance of particle-driven currents reported by *Hallworth and Huppert* [1998] and the length scale $(g'A^5/\nu^2)^{1/7}$ (Figure 10). (Viscosities for silicon carbide (SiC) slurries were calculated using a modified Kreiger and Dougherty model, as suggested by rheological measurements by *Ferreira and Diz* [1999]). This result suggests that the abrupt transitions occur in both solute-driven laboratory flows and particle-driven laboratory

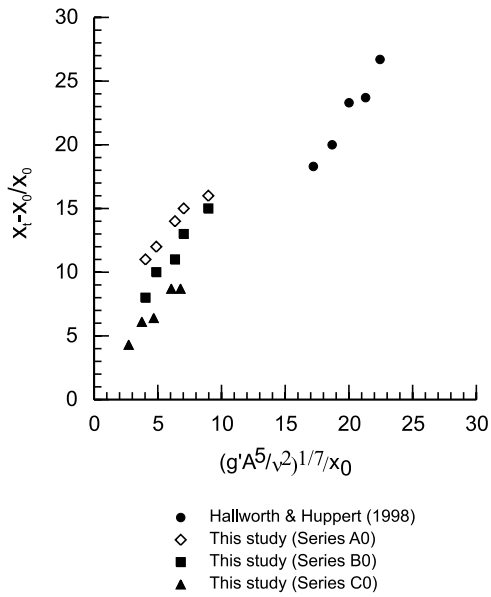


**Figure 10.** Dimensionless abrupt transitions distance $x_t - x_0/x_0$ as a function of the dimensionless scaling parameter $(g'A^5/\nu^2)^{1/7}/x_0$.

**Table 2.** Critical Reynolds Numbers for Abrupt Transitions[a]

| Experimental Series | Predicted | Empirical |
|---|---|---|
| This study (series A0) | 215 | $Re > 850$ |
| This study (series B0) | 215 | $530 > Re < 1225$ |
| This study (series C0) | 488 | $680 > Re < 1727$ |
| *Hallworth and Huppert* [1998] | 65 | $5500 > Re < 7397$ |

[a]Comparison between the critical Reynolds numbers, below which currents should undergo an abrupt transition, predicted by equation (11) and those determined empirically.

currents for the same reason, i.e., a dynamic change in flow regime. It also implies that particle settling was not important in determining the occurrence and location of the abrupt transition in *Hallworth and Huppert* [1998] experiments. This conclusion may also be deduced by evaluating the magnitude of the particle settling velocity ($\omega_s$) compared to the flow duration (Table 3). In addition, the Silicon Carbide (SiC) slurries used by *Hallworth and Huppert* [1998] are non-Newtonian fluids with shear thinning properties and exhibit a yield strength which is ~950 Pa at concentrations of ~0.34Ø [*Ferreira and Diz*, 1999; *Sun and Gao*, 2001]. The non-Newtonian suspension properties, apparently, did not significantly influence the abrupt transition distance. Although prediction of the abrupt transitions distance agrees with the scaling theory, we find a significant difference between the Reynolds number at which these particle-driven currents should first display abrupt transitions, calculated using equation (11) and the Reynolds number estimated using the initial flow parameters (Table 2). This could be related to problems of accurately predicting the suspension viscosity using the modified *Kreieger and Dougherty* [1959] model.

### 5.3. Cloud Buoyancy

[30] The generation of a low-concentration cloud in experiments is intimately linked to mixing within the current prior to the abrupt deceleration. Mixing at the front and top of the flow forms a vertically stratified current with a relatively dense and more viscous, unmixed or poorly mixed lower region and a more dilute upper region. The abrupt transition occurs at the point where the unmixed fluid undergoes a change in flow regime from inertial-slumping to viscous-buoyancy spreading, but it is also the point where the unmixed and mixed regions of the current move independently and under different dynamical regimes. Hence these currents may be considered as comprising two distinct flows; a slower moving lower region spreading under a viscous-buoyancy regime and an upper cloud spreading under an inertial-buoyancy regime.

[31] Commonly a bulk Richardson number, $Ri = 1/Fr^2$, is used to measure mixing in gravity flows. This approach is appropriate only for turbulent currents [*Ellison and Turner*, 1959]. Hence it is unsurprising that in this study there is a poor correlation between the bulk Richardson number and the observed degree of mixing in the low Reynolds numbers flows (Table 1). It has been found for currents with low Reynolds numbers that there is a strong dependency of mixing on the Reynolds number. Mixing is enhanced at larger Reynolds numbers [*Britter and Simpson*, 1978; *García and Parsons*, 1996; *Parsons and García*, 1998].

[32] A proxy for mixing in currents that undergo abrupt transitions may be evaluated by considering the current's buoyancy, a measure of its excess density and volume, $B = g'A$ [*Gladstone et al.*, 2004]. The ratio of the current's buoyancy during the inertial-buoyancy spreading phase to the initial current buoyancy, $\beta = B_i/B_0$, gives an indication of the proportion of the initial buoyancy involved in driving the motion of the mixed cloud. If $\beta = 1$, all of the initial buoyancy is involved in driving the current during the inertial-buoyancy spreading phase, thus there is no partitioning of the current's initial buoyancy. When $\beta < 1$, only some of the initial buoyancy is involved in driving the cloud and thus the current's initial buoyancy is partitioned between the cloud and the unmixed high-concentration region. The buoyancy during the inertial-buoyancy spreading phase for laboratory currents was calculated using a rearranged form of equation (2):

$$B_i = g'A = \left(\frac{x}{(3/2Fr)^{2/3}t^{2/3}}\right)^3. \quad (12)$$

**Table 3.** Starting Conditions of *Hallworth and Huppert*'s [1998] Particle-Laden Experiments[a]

| Name | $\gamma$ | $x_0$, m | $H_0$, m | $g'$, ms$^{-2}$ | Ø | $\rho$, k g m$^{-3}$ | $\mu$, kg m$^{-1}$ s$^{-1}$ | $\nu$, m$^2$ s$^{-1}$ $\times 10^{-6}$ | $u_i$, m s$^{-1}$ | $Re$ | Fr | $\omega_s$, mm s$^{-1}$ | $\rho$* |
|---|---|---|---|---|---|---|---|---|---|---|---|---|---|
| Expt 28 | 0 | 0.03 | 0.1 | 0.54 | 0.025 | 1055.5 | 0.00114 | 1.1 | 0.09 | 8333 | 0.40 | 0.0728 | 0.18 |
| Expt 40 | 0 | 0.03 | 0.1 | 3.26 | 0.150 | 1332.8 | 0.00243 | 1.8 | 0.24 | 13163 | 0.41 | 0.0167 | 0.38 |
| Expt 29 | 0 | 0.03 | 0.1 | 5.44 | 0.250 | 1554.6 | 0.00522 | 3.4 | 0.29 | 8637 | 0.39 | 0.0040 | 0.47 |
| Expt 43 | 0 | 0.03 | 0.1 | 5.98 | 0.275 | 1610.1 | 0.00653 | 4.1 | 0.30 | 7397 | 0.39 | 0.0025 | 0.49 |
| Expt 38[b] | 0 | 0.03 | 0.1 | 6.52 | 0.300 | 1665.5 | 0.00830 | 5.0 | 0.27 | 5418 | 0.34 | 0.0017 | 0.50 |
| Expt 42[b] | 0 | 0.03 | 0.1 | 7.07 | 0.325 | 1721.0 | 0.01077 | 6.3 | 0.28 | 4474 | 0.33 | 0.0010 | 0.52 |
| Expt 30[b] | 0 | 0.03 | 0.1 | 7.61 | 0.350 | 1776.4 | 0.01430 | 8.0 | 0.30 | 3727 | 0.35 | 0.0007 | 0.53 |
| Expt 41[b] | 0 | 0.03 | 0.1 | 8.15 | 0.375 | 1831.9 | 0.01951 | 10.7 | 0.27 | 2535 | 0.30 | 0.0004 | 0.55 |
| Expt 39[b] | 0 | 0.03 | 0.1 | 8.70 | 0.400 | 1887.3 | 0.02754 | 14.6 | 0.15 | 1028 | 0.16 | 0.0002 | 0.56 |

[a]Variables are the channel slope gradient ($\gamma$), lock length ($x_0$) and height ($h_0$), reduced gravity ($g'$), volumetric particle concentration fraction (Ø), density ($\rho$), viscosity ($\mu$), kinematic viscosity ($\nu$), initial head velocity ($u_i$), calculated Reynolds ($Re$) and Froude ($Fr$) numbers, particle settling velocity ($\omega_s$), and the density ratio ($\rho$*). The current's density was calculated using, $\rho = Ø\rho_p + (1 - Ø)\rho_a$, where Ø is the initial particle volume fraction, $\rho_p$ is the density of particles used, and $\rho_a$ is the density of the ambient fluid. The viscosity of particle-water mixtures was estimated using a modified *Kreieger and Dougherty* [1959] model for viscosity valid for shear rates of 10 s$^{-1}$ [*Ferreira and Diz*, 1999], where $\mu/\mu_w = (1 - Ø/Ø_m)^{-3.2}$, where $\mu$ and $\mu_w$ are the dynamic viscosity of the particle-water mixture and water, respectively, Ø is the volumetric sediment concentration, and $Ø_m$ is the maximum packing concentration of ~0.62. The flows of *Hallworth and Huppert* [1998] can be estimated to have had shear rates ($\gamma = \partial u/\partial y$) of the order of 10 s$^{-1}$, given head velocities of ~0.2 m s$^{-1}$ and a height above the bed of the velocity maximum of ~1 cm. The Reynolds and Froude numbers were calculated using the same method described in the caption to Table 1. The settling velocity of particles was estimated using the equation proposed by *Richardson and Zaki* [1954] for concentrated particulate suspensions.

[b]Experiments in which an abrupt transition was observed.

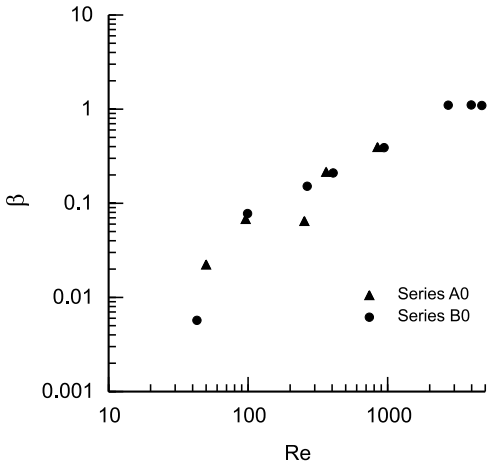


**Figure 11.** Parameter β indicating the ratio of the current's buoyancy during the inertial-spreading phase to the initial buoyancy against Reynolds number. See text for explanation.

A Froude number equal to unity was used, since this value was found to be appropriate to describe the motion of currents that did not undergo an abrupt transition (i.e., using equation (2)). Furthermore, this value is appropriate for flow with small thicknesses relative to the ambient depth [*Huppert and Simpson*, 1980]. The values of β for experiments are shown against Reynolds number in Figure 11. Experimental currents that did not experience an abrupt transition, with $Re > 2000$, have values $\beta \sim 1$ indicating no partitioning of the initial buoyancy. Currents that exhibited an abrupt transition, with $Re < 2000$, however, show a strong correlation of β with Reynolds number. This indicated that the buoyancy in these currents was strongly partitioned at the time the cloud formed the flow front. A smaller fraction of the current's buoyancy was involved in driving the cloud with decreasing *Re*. For example, at $Re \sim 100$ the cloud had a buoyancy of one tenth that of the initial current's buoyancy. The relationship between β and Reynolds number suggests a positive correlation between Reynolds number and amount of mixing, concurring with previous studies [*Britter and Simpson*, 1978; *García and Parsons*, 1996; *Parsons and García*, 1998].

[33] It was also found that the time between the abrupt deceleration of high-concentration fluid and the development of an inertial-spreading cloud, $t_\lambda$, decreased markedly with Reynolds number (Figure 12). This observation can also be interpreted as a consequence of mixing in currents and the cloud buoyancy. Relatively high-Reynolds-number currents produce voluminous clouds with large buoyancies that continue downstream almost immediately after the abrupt transition. In contrast, relatively low-Reynolds-number currents produce clouds with much smaller buoyancies that do not immediately overtake the arrested flow front. Hence variations in mixing can explain why currents display a progressive change in their pattern of motion from "strong" to "weak" abrupt transitions as Reynolds number increases (Figures 6a and 6b). Since existing theoretical models for the motion of density currents ignore mixing, this limits their application to currents that undergo abrupt transitions in which mixing plays an important role in determining the current's motion.

### 5.4. Influence of Slope Gradient

[34] Experiments indicate that a relatively small change in slope can be responsible for a significant change in the distance at which currents experience transitions in flow dynamic regimes (Figure 7). Slope can also alter the dynamic regimes through which currents progress, by altering the amount of mixing currents experience. For currents with low viscosity and high Reynolds numbers the transition distance from inertial slumping to inertial spreading is linearly dependent on slope and increases by a factor of about two over a 5° change in gradient (Figure 13a). For high-viscosity, low-Reynolds-number currents, the abrupt transition distance between inertial slumping and viscous spreading is again linearly dependent on slope angle. The abrupt transition distance, however, increases threefold over a 5° gradient change (Figure 13b). It was observed that currents on larger slopes underwent more mixing and the cloud's buoyancy was therefore enhanced. Hence the abrupt transitions in currents of the same starting density and viscosity were observed to become progressively weaker, i.e., the cloud was more vigorous and overtook the flow front more rapidly, as slope increased (Figure 7c).

## 6. Discussion

### 6.1. Dynamic Similarity of Natural Flows

[35] This study has identified that abrupt transitions occur in laboratory solute- and particle-driven density currents due to a change in dynamical regime from inertial-slumping to viscous-buoyancy spreading. However, do abrupt transitions occur in much larger natural currents for the same reason? A straightforward comparison between laboratory and natural currents is problematic since not all aspects of natural flows are modeled in the laboratory experiments. Furthermore, the nature of the laboratory experiments means that our analysis is only valid for flows that are moving sufficiently rapidly that their inertia is nonnegligible. This is likely to be the case for sudden, large-scale, catastrophic collapses that might be initiated by

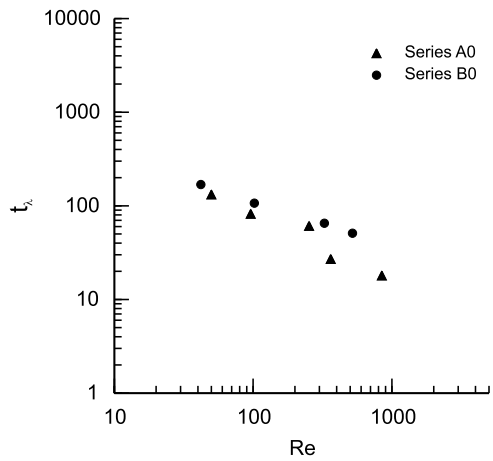


**Figure 12.** Time taken after the abrupt transition for the dilute cloud to display inertial spreading, when *x* changes with $t^{2/3}$, $t_\lambda$, plotted against Reynolds number.

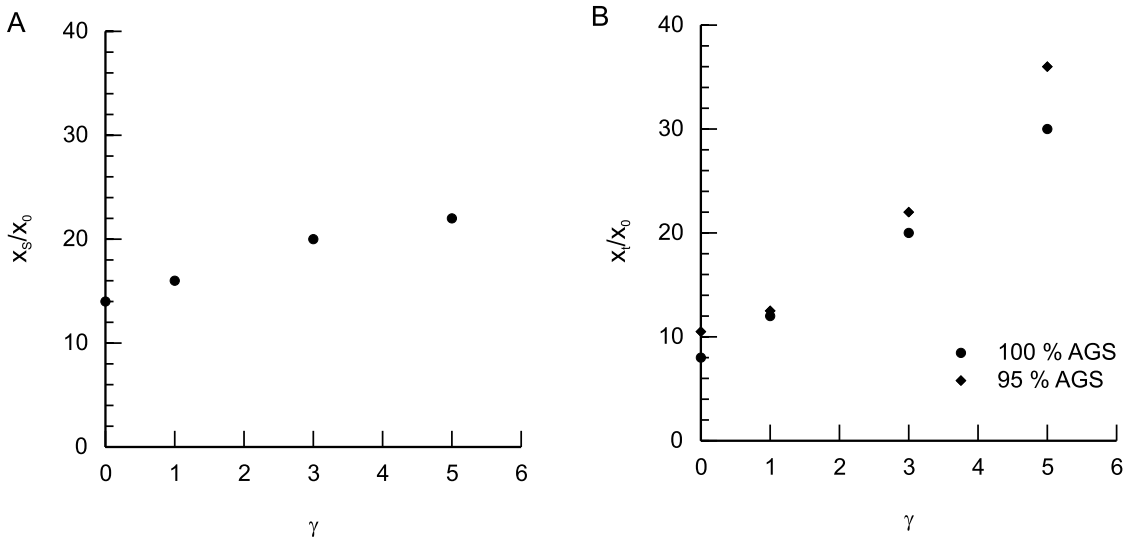


**Figure 13.** Effect of slope gradient, γ, on (a) the transition distance from intertial slumping to inertial buoyancy spreading regimes and (b) the abrupt transition distance.

earthquakes or volcanic eruptions, but will not necessarily be true for gravity currents generated by other mechanisms. Additionally, it is possible that currents generated by lock release initially have an enhanced inertial slumping phase compared to natural flows as a result of the strong return flow of ambient fluid.

[36] Bearing in mind the above points we discuss some implications of the scaling analysis presented above. Equation (11) indicates that abrupt transitions should only be observed in currents with sufficiently small Reynolds numbers. The "critical Reynolds" number for an abrupt transition depends on the initial aspect ratio; given currents with $h_0/x_0$ of ~0.1 and 10, only those flows with Reynolds numbers less than ~2000 and 22 will exhibit abrupt transitions, respectively. These values are relatively small compared to those for natural currents with much larger thicknesses and velocities. For example, *Kneller and Buckee* [2000] estimate that subaqueous sand-laden flows with a fractional concentration of 0.45 will have Reynolds number >2000 when the product of velocity and thickness exceed $3 \times 10^{-2}\ m^2\ s^{-1}$. Hence given that most natural currents will be characterized by large Reynolds numbers, greater than the critical Reynolds number, it follows that most natural flows should not undergo an abrupt transition in the same manner as the laboratory currents studied. Although this seems a relatively straightforward conclusion, the analysis of Reynolds numbers for natural flows and particularly for those with high concentrations is problematic since it is often difficult to determine meaningful values of flow properties. The effective viscosity as well as the effect of turbulence suppression caused by high particle concentrations is particularly poorly constrained [*Branney and Kokelaar*, 2002]. Future laboratory experiments may be employed to test empirically if currents with high particle concentrations and high Reynolds numbers undergo an abrupt transition.

### 6.2. Other Mechanisms for Abrupt Transitions

[37] The process of decoupling in pyroclastic flows [*Yamamoto et al.*, 1993; *Fisher*, 1995; *Fujii and Nakada*, 1999; *Bourdier and Abdurachman*, 2001; *Cole et al.*, 2002] and snow avalanches [*Issler*, 2003] is similar in many respects to the abrupt transition behavior of laboratory experiments; the slowing of a high-concentration basal layer and outrunning by a dilute cloud. Given that the mechanism that causes abrupt transitions in laboratory currents may not operate in natural flows, we now consider what other mechanisms might be responsible for abrupt transitions. In several examples of natural flows it is inferred that decoupling is induced by topography. This seems likely since the dense and dilute parts of current are affected differently by topography [*Fisher*, 1995]. *Bourdier and Abdurachman* [2001] found that a primary site of decoupling of pyroclastic flows running down the flanks of the Merapi volcano in Indonesia was a topographic break-in slope. The slope break may be interpreted to have induced the rapid deceleration of the dense underflow and allowed the cloud to decouple. This gradient-related mechanism has also been postulated by *Denlinger* [1987]. Alternatively, it can be envisaged that decoupling might occur in the absence of a gradient change [*Fisher*, 1995]. The dilute cloud could obtain a larger buoyancy than that of the dense underflow, which for example, might occur in flows that undergo large amounts of mixing or elutriation of fines. In this case the dilute cloud could accelerate away from the parental dense flow without, necessarily, an associated abrupt deceleration of the underlying dense layer. This buoyancy-driven decoupling has been demonstrated indirectly using laboratory experiments on buoyancy-stratified flows [*Gladstone et al.*, 2004]. Similarly, a decrease in the dense layer's buoyancy could induce an abrupt transition, for example as it thins due to progressive sedimentation. Another model involves changing near-bed concentration. An increase in the near-bed concentration could cause local deceleration due to enhanced friction between particles and effective viscosity. This process might occur during rapid sedimentation or substrate erosion (see discussion by *Fisher* [1995]). Such stratified currents, with viscously controlled near bed regions, have been demonstrated using experiments [cf. *Amy et al.*, 2005a, 2005b]. Future studies should focus on constraining how the run-out length of the dense

flow and dilute cloud is controlled by abrupt transitions, when caused by these other mechanisms.

### 6.3. Stepped Thickness Patterns

[38] Experiments by *Hallworth and Huppert* [1998] show that laboratory currents that undergo an abrupt transition produce beds with a step-like geometry (Figure 1b). *Kneller and Buckee* [2000] pointed out that this "stepped geometry" is similar to those found for the deposits of submarine flow within the Mio-Pliocene of Japan [*Hirayama and Nakajima*, 1977; *Tokuhashi*, 1979]. These beds were deposited in a relatively low-gradient basin plain environment. More recently, work on Miocene submarine flow deposits of Italy, deposited in a similar depositional environment, has revealed similar bed geometries [*Talling et al.*, 2004; *Amy et al.*, 2005a, 2005b]. In both of these examples the reduction in sandstone thickness occurs over a short distance, 5 km or less, relative to the overall bed length of several tens to several hundreds of kilometers.

[39] The geometry of deposits mapped in outcrops suggests that natural submarine currents may also undergo rapid changes in flow dynamics to produce stepped deposit thickness patterns. However following the reasoning outlined above, abrupt transitions in natural and laboratory currents are unlikely to be caused by the same mechanism. The natural flow deposits described were deposited on relatively flat basin floors. Thus if flows underwent an abrupt deceleration because of a change in gradient, it implies that only small gradients (<1°) are necessary for this to occur [cf. *Wynn et al.*, 2002]. Submarine currents often carry cohesive sediment. The effect of changes in flow concentration in these flows is therefore likely to be important since small increases in clay content can dramatically change the effective "fluid" viscosity and yield strength [e.g., *Coussot*, 1997]. As a result, these flows could be especially prone to transformation by erosion and bulking or deceleration and loss of turbulence. Quantifying the effects of mud concentration on flow transformation is an important area of future research.

### 6.4. Implications for Physical Modeling

[40] This study has a number of important implications for the physical modeling of density currents. First, gravity currents have traditionally been studied using the lock exchange mechanism, however, this study illustrates that although certain aspects of laboratory current behavior may be qualitatively similar to natural flows, in fact, they might be dynamically dissimilar. One aspect of particular importance is the rapid release of fluid from a lock. This "dam break" generation mechanism may not be fully representative of many natural particle-laden gravity currents due to the inertial slumping that is enhanced by the initial return flow of ambient fluid. It is therefore suggested that other techniques for generating density currents (e.g., using an external input tank) may be more appropriate for modeling currents [e.g., *Peakall et al.*, 2001]. Secondly, it is possible that previous laboratory studies have overlooked the "abrupt transition" behavior of density currents, especially since under certain conditions it can be weakly developed. This could make the results from some laboratory studies difficult to interpret; if and by how much was flow behavior and sedimentation influenced by the abrupt transition process? Hence future laboratory studies using the lock exchange method should be careful to assess the role of abrupt transitions on their results.

## 7. Conclusions

[41] The abrupt transition behavior of surge-type, laboratory density currents has been studied to investigate why this behavior occurs in laboratory flows and if a similar mechanism for abrupt transitions will operate in natural particle-laden currents. The new experiments show that solute-driven density currents undergo abrupt transitions as well as particle-laden flows, for example those previously reported by *Hallworth and Huppert* [1998]. Results show that currents that display an abrupt transition have relatively low Reynolds numbers and $Re < 2000$ for solute driven flows of this study. The distance at which an abrupt transition occurs for currents with different initial densities, viscosities and aspect ratios, either with or without particles, is proportional to the length scale between the inertia-buoyancy and viscous-buoyancy regimes. This finding implies that abrupt transitions occur due to a dynamic change between these two regimes, even though the spreading patterns of currents appear to indicate a change directly from inertial-slumping to viscous-buoyancy spreading, where currents' lengths increase by $t^1$ and $t^{-1/5}$, respectively. We interpret that in these currents, the timescales of the onset of inertia buoyancy, $t_1$, and viscous buoyancy, $t_2$, are comparable and thus the inertia-buoyancy phase is very short lived and hence difficult to observe. The ratio of the timescales $t_1$ and $t_2$ is a function of the flow Reynolds number and its initial aspect ratio (equation (11)). Hence abrupt transitions, caused by the described change in dynamic regime, should occur below a critical Reynolds number, whose value depends on the initial aspect ratio. Flows in nature typically have relatively high Reynolds numbers, with values exceeding those of the critical Reynolds numbers. On this basis, it seems likely that abrupt transitions in natural currents will not be caused by the same mechanism identified for the laboratory flows but will occur due to some other mechanisms. However, we recognize that using a Reynolds number to characterize the dynamics of high-concentration, particle-laden flow is problematic. Future work should aim to quantify other mechanisms by which abrupt transitions could occur (e.g., slope gradient change) and document how they affect the run-out distance and the depositional patterns of currents.

## Notation

- $A$ area of the gravity current (i.e., volume per unit width), $m^2$.
- $\alpha_0$ initial aspect ratio of the current, dimensionless.
- $\beta$ current's buoyancy during the inertial spreading phase compared as a ratio of the initial buoyancy, dimensionless.
- $B_0$ current's initial buoyancy, $m^3/s^2$.
- $B_i$ current's buoyancy during the inertial spreading phase, $m^3/s^2$.
- Ø particle fractional concentration by volume, dimensionless.
- $Fr$ Froude number, dimensionless.

$g'$ current's reduced gravity, m/s$^2$.
$\gamma$ slope gradient, deg.
$h_0$ current's initial height, m.
$H$ ambient fluid depth, m.
$k$ coefficient of velocity during the inertial slumping regime, dimensionless.
$\mu$ dynamic viscosity, kg/m s.
$\nu$ kinematic viscosity, m$^2$/s.
$\omega_s$ particle settling velocity in a high-concentration suspension, m/s.
$\nu_s$ particle settling velocity in a low-concentration suspension, m/s.
$Re$ Reynolds number, dimensionless.
$Ri$ Richardson number, dimensionless.
$\rho_a$ ambient fluid density, kg/m$^3$.
$\rho_f$ flow density, kg/m$^3$.
$\rho_p$ particle density, kg/m$^3$.
$\rho^*$ initial density ratios, dimensionless
$t$ time, s.
$t_\lambda$ time taken for a dilute cloud to display inertial spreading after an abrupt transition, s.
$u_i$ current velocity in the inertial slump phase, m/s.
$x$ current's length, m.
$x_0$ initial current length, m.
$x_s$ current's length at the transition from inertial slumping to inertial buoyancy regimes, m.
$x_*$ current's length at the transition from inertial buoyancy to viscous buoyancy regimes, m.
$x_t$ current's length at the transition from inertial slumping to inertial viscous regimes, m.

[42] **Acknowledgments.** Research was funded by the United Kingdom Natural Environmental Research Council and Conoco (now ConocoPhillips) through the OCEAN MARGINS-LINK scheme (grant NER/T/S/2000/01403). Funding for the laboratory facilities used was provided by EPSRC (GR/R60843/01) and by a consortium of oil companies including BG, BHP, Chevron Texaco, Total, Exxon Mobil, ConocoPhillips, Amerada Hess, and Shell. The authors are grateful to Richard Iverson and Jeffrey Parsons for careful reviews and to Caroline Choux, Maarten Felix, Charlotte Gladstone, Chris Keylock, Jeremy Philips, Sarah Nield, and Steve Sparks for valuable discussion. Mark Franklin, Maarten Felix, Rufus Brunt, and Gareth Keevil kindly helped run laboratory experiments. Mark Hallworth and Herbert Huppert are thanked for sharing their experimental data shown in Figure 1.

## References

Amy, L. A., P. J. Talling, J. Peakall, R. B. Wynn, and R. G. Arzola Thynne (2005a), Bed geometry used to test recognition criteria of turbidites and (sandy) debrites, *Sediment. Geol.*, in press.

Amy, L. A., J. Peakall, and P. J. Talling (2005b), Evolution of density- and viscosity-stratified gravity currents: Insight from physical experiments and implications for submarine flow deposits, *Sediment. Geol.*, in press.

Bagnold, R. A. (1954), Experiments on a gravity-free dispersion of large solid spheres in a Newtonian fluid under shear, *Philos. Trans. R. Soc. London, Ser. A*, *225*, 49–63.

Barnes, H. A. (1989), Shear-thickening ("dilatancy") in suspensions of nonaggregating solid particles dispersed in Newtonian liquids, *J. Rheol.*, *33*, 329–366.

Benjamin, T. B. (1968), Gravity currents and related phenomena, *J. Fluid Mech.*, *31*, 209–248.

Bonnecaze, R. T., H. E. Huppert, and J. R. Lister (1993), Patterns of sedimentation from polydispersed turbidity currents, *Proc. R. Soc. London*, *452*, 2247–2261.

Bourdier, J. L., and E. K. Abdurachman (2001), Decoupling of small-volume pyroclastic flows and related hazards at Merapi volcano, Indonesia, *Bull. Volcanol.*, *63*, 309–325.

Branney, M. J., and P. Kokelaar (2002), *Pyroclastic Density Currents and the Sedimentation of Ignimbrites*, *Geol. Soc. London Mem.*, vol. 27, 143 pp., Geol. Soc. of London, U. K.

Britter, R. E., and J. E. Simpson (1978), Experiments on the dynamics of a gravity current head, *J. Fluid Mech.*, *88*, 233–240.

Chen, Y. M., and A. J. Pearlstein (1987), Viscosity-temperature correlation for glycerol-water solutions, *Indust. Eng. Chem. Res.*, *26*, 1670–1672.

Choux, C. M. (2001), Sedimentation et segregation dans les ecoulements de suspension concentree: Approche experimentale et applications volcanolgiques, Ph.D. thesis, *number 304*, 214 pp., Univ. Blaise Pascal, Clermont-Ferrand, France.

Choux, C. M., and T. H. Druitt (2002), Analogue study of particle segregation in pyroclastic density currents, with implications for the emplacement mechanisms of large ignimbrites, *Sedimentology*, *49*, 907–928.

Cole, P. D., E. S. Calder, R. S. J. Sparks, A. B. Clarke, T. H. Druitt, S. R. Young, R. A. Herd, C. L. Harford, and E. E. Norton (2002), Deposits from dome-collapse and fountain collapse pyroclastic flows at Soufriere Hills Volcano, Montserrat, in *The Eruption of Soufriere Hills Volcano, Montserrat, From 1995 to 1999*, *Geol. Soc. London Mem.*, vol. 21, edited by T. H. Druitt and B. P. Kokelaar, pp. 231–262, Geol. Soc. of London, U. K.

Coussot, P. (1997), *Mudflow Rheology and Dynamics*, 270 pp., Delft Hydraul., Int. Assoc. for Hydraul. Res., Delft, Netherlands.

Dade, W. B., and H. E. Huppert (1995), Runout and fine-sediment deposits of axisymmetric turbidity currents, *J. Geophys. Res.*, *100*, 18,597–18,609.

Denlinger, R. P. (1987), A model for generation of ash clouds by pyroclastic flows, with application to the 1980 eruptions at Mount St. Helens, Washington, *J. Geophys. Res.*, *92*, 10,284–10,298.

Ellison, T. H., and J. S. Turner (1959), Turbulent entrainment in stratified flows, *J. Fluid Mech.*, *6*, 423–448.

Ferreira, J. M., and H. M. Diz (1999), Effect of solids loading on slip-casting performance of silicon carbide slurries, *J. Am. Ceramic Soc.*, *82*, 1993–2000.

Fisher, R. V. (1995), Decoupling of pyroclastic currents—Hazards assessments, *J. Volcanol. Geotherm. Res.*, *66*, 257–263.

Fujii, T., and S. Nakada (1999), The 15 September 1991 pyroclastic flow at Unzen Volcano (Japan): A flow model for associated ash-cloud surges, *J. Volcanol. Geotherm. Res.*, *89*, 159–172.

García, M. H., and J. D. Parsons (1996), Mixing at the front of gravity currents, *Dyn. Atmos. Oceans*, *24*, 197–205.

Gladstone, C., and A. W. Woods (2000), On the application of box models to particle-driven gravity currents, *J. Fluid Mech.*, *416*, 187–195.

Gladstone, C., L. J. Ritchie, R. S. J. Sparks, and A. W. Woods (2004), An experimental investigation of stratified inertial gravity currents, *Sedimentology*, *51*, 767–789.

Gröbelbauer, H. P., T. K. Fanneløp, and R. E. Britter (1993), The propagation of intrusion fronts of high density ratios, *J. Fluid Mech.*, *250*, 669–687.

Hallworth, M. A., and H. E. Huppert (1998), Abrupt transitions in high-concentration, particle-driven gravity currents, *Phys. Fluids*, *10*, 1083–1087.

Hampton, M. A. (1972), The role of subaqueous debris flow in generating turbidity currents, *J. Sediment. Petrol.*, *42*, 775–793.

Harris, T. C., A. J. Hogg, and H. E. Huppert (2002), Polydisperse particle-driven gravity currents, *J. Fluid Mech.*, *472*, 333–371.

Heezen, B. C., and M. Ewing (1952), Turbidity current and submarine slump, and the 1929 Grand Banks earthquake, *Am. J. Sci.*, *250*, 849–873.

Heezen, B. C., and M. Ewing (1955), Orleansville earthquake and turbidity current, *AAPG Bull.*, *39*, 2505–2514.

Hirayama, J., and N. Nakajima (1977), Analytical study of turbidites, Otadai Formation, Boso Peninsula, Japan, *Sedimentology*, *24*, 747–779.

Huppert, H. E. (1982), The propagation of two-dimensional and axisymmetric viscous gravity currents over a rigid horizontal surface, *J. Fluid Mech.*, *121*, 43–58.

Huppert, H. E., and J. E. Simpson (1980), The slumping of gravity currents, *J. Fluid Mech.*, *99*, 785–799.

Issler, D. (2003), Experimental information on the dynamics of dry snow avalanches, in *Dynamic Response of Granular and Porous Materials Under Large Catastrophic Deformation*, *Lecture Notes Appl. Comput. Mech.*, vol. 2, edited by K. Hutter and N. Kitcher, pp. 109–160, Springer, New York.

Keulegan, G. H. (1957), An experimental study of the motion of saline water from locks into fresh water channels, *Rep. 5168*, U.S. Natl. Bur. of Standards, Gaithersburg, Md.

Klemp, J. B., R. Rotunno, and W. C. Skamarock (1994), On the dynamics of gravity currents in a channel, *J. Fluid Mech.*, *269*, 169–198.

Kneller, B., and C. Buckee (2000), The structure and fluid mechanics of turbidity currents: A review of some recent studies and their geological implications, *Sedimentology*, *47*, 62–94.

Kreieger, I. M., and T. J. Dougherty (1959), A mechanism for non-Newtonian flow in suspension of rigid spheres, *Trans. Soc. Rheol.*, *3*, 137–152.

Lide, D. L., G. Baysinger, L. I. Berger, R. N. Goldberg, H. V. Kehiaian, K. Kuchitsu, C. C. Lin, G. Rosenblatt, and A. L. Smith (2004), *CRC Handbook of Chemistry and Physics*, 84th ed., CRC Press, Boca Raton, Fla.

Lube, G., H. E. Huppert, R. S. J. Sparks, and M. A. Hallworth (2004), Axisymmetric collapses of granular columns, *J. Fluid Mech.*, *508*, 175–199.

Luthi, S. (1981), Some new aspects of two-dimensional turbidity currents, *Sedimentology*, *28*, 97–105.

Major, J. J., and T. C. Pierson (1992), Debris flow rheology: Experimental analysis of fine-grained slurries, *Water Resour. Res.*, *28*, 841–857.

Middleton, G. V., and W. J. Neal (1989), Experiments on the thickness of beds deposited by turbidity currents, *J. Sediment. Petrol.*, *59*, 297–307.

Mohrig, D., and J. G. Marr (2003), Constraining the efficiency of turbidity current generation from submarine debris flows and slides using laboratory experiments, *Mar. Pet. Geol.*, *20*, 883–899.

Morgenstern, N. R. (1967), Submarine slumping and the initiation of turbidity currents, in *Marine Geotechniques*, edited by A. Richards, pp. 189–220, Univ. of Ill. Press, Urbana.

Mulder, T., B. Savoye, and J. P. M. Syvitski (1997), Numerical modeling of a mid-sized gravity flow: The 1979 Nice turbidity current (dynamics, processes, sediment budget and seafloor impact), *Sedimentology*, *44*, 305–326.

Parsons, J. D., and M. H. García (1998), Similarity of gravity current fronts, *Phys. Fluids*, *10*, 3209–3213.

Peakall, J., M. Felix, W. D. McCaffrey, and B. Kneller (2001), Particulate gravity currents: Perspectives, in *Particulate Gravity Currents*, *Spec. Publ. 31*, edited by W. D. McCaffrey, B. C. Kneller, and J. Peakall, pp. 1–8, Intl. Assoc. of Sediment., Santa Barbara, Calif.

Piper, D. J. W., P. Cochonat, and M. L. Morrison (1999), The sequence of events around the epicenter of the 1929 Grand Banks earthquake: Initiation of debris flows and turbidity current inferred from sidescan sonar, *Sedimentology*, *46*, 79–97.

Richardson, J. F., and W. N. Zaki (1954), Sedimentation and fluidization: part I, *Trans. Inst. Chem. Eng.*, *32*, 35–53.

Rooij, F. D. E., and S. B. Daziel (2001), Time- and space-resolved measurements of deposition under turbidity currents, in *Particulate Gravity Currents*, *Spec. Publ. 31*, edited by W. D. McCaffrey, B. C. Kneller, and J. Peakall, pp. 207–215, Intl. Assoc. of Sediment., Santa Barbara, Calif.

Rottman, J. W., and J. E. Simpson (1983), Gravity currents produced by instantaneous releases of heavy fluid in a rectangular channel, *J. Fluid Mech.*, *135*, 95–110.

Schmidt, W. (1911), Zur Mechanik der Boewn, *Z. Meterol*, *28*, 355–362.

Simpson, J. E. (1997), *Gravity Currents in the Environment and the Laboratory*, 2nd ed., 244 pp., Cambridge Univ. Press, New York.

Sun, J., and L. Gao (2001), Dispersing SiC powder and improving its rheological behavior, *J. Eur. Ceramic Soc.*, *21*, 2447–2451.

Talling, P. J., L. A. Amy, R. B. Wynn, J. Peakall, and M. Robinson (2004), Beds comprising debrite sandwiched within cogenetic turbidite, *Sedimentology*, *51*, 163–194.

Tokuhashi, S. (1979), Three-dimensional analysis of a large sandy-flysch body, Mio-Pliocene Kiyosumi Formation, Boso Peninsula, Japan, in *Memoirs of the Faculty of Science*, *Ser. Geol. Mineral.*, vol. 46, pp. 1–60, Kyoto Univ., Japan.

van der Knaap, W., and R. Eijpe (1968), Some experiments on the genesis of turbidity currents, *Sedimentology*, *11*, 115–124.

Weimer, P., and M. H. Link (1991), Global petroleum occurrences in submarine fans and turbidite systems, in *Seismic Facies and Sedimentary Process of Submarine Fans and Turbidite Systems*, edited by P. Weimer and M. H. Link, pp. 9–67, Springer, New York.

Wynn, R. B., P. P. E. Weaver, D. G. Masson, and D. A. V. Stow (2002), Turbidite depositional architecture across three inter-connected deep-water basins on the Northwest African Margin, *Sedimentology*, *49*, 669–695.

Yamamoto, T., S. Takarada, and S. Suto (1993), Pyroclastic flows from the 1991 eruption of Unzen Volcano, *Jpn. Bull. Volcanol.*, *55*, 166–175.

L. A. Amy and P. J. Talling, Department of Earth Sciences, Centre for Environmental and Geophysical Flows, University of Bristol, Bristol BS8 1RJ, UK. (l.amy@bristol.ac.uk; peter.talling@bristol.ac.uk)

A. J. Hogg, School of Mathematics, Centre for Environmental and Geophysical Flows, University of Bristol, Bristol BS8 1RJ, UK. (a.j.hogg@bristol.ac.uk)

J. Peakall, Earth and Biosphere Institute, School of Earth and Environment, University of Leeds, Leeds, LS2 9JT, UK. (jeffrey@earth.leeds.ac.uk)